University of Stavanger

Faculty of Science and Technology

MASTER'S THESIS

Study program/Specialization: Petroleum Engineering, Drilling and Well Technology	Spring semester, 2016 Open
Writer: Svein Kåre Malo Dahle	…… (Writer's signature)
Faculty supervisor: Jan Aage Aasen	
Thesis title: A simple model for predicting the internal and external filtration during produced water re-injection using field data from Grane well G-32.	
Credits (ECTS): 30	
Key words: PWRI Internal filtration External filtration Produced water Filtration coefficient Formation damage coefficient Separation methods Produced water management	Pages: 70 + enclosure: 3 Stavanger, 14/06/2016

Abstract

Produced water re-injection is a method for managing the produced water in an environmentally friendly way by injecting produced water into a porous formation. This is also a method of maintaining the reservoir pressure. Contaminations in the injected water will reduce the injectivity by plugging the porous media around the borehole and by creating an external filter cake, effectively reducing the porosity and permeability. The first stage of injectivity decline is internal filtration, and is when solids get deposited in the area close to the borehole. The second stage is external filtration, and this is when particles no longer penetrate into the formation, but start forming an external filter cake

The thesis presents a model for the impedance, which is the inverse of the injectivity, that takes into account the internal and external filtration. This model is tested using field data from Grane well G-32. Grane has a high porosity and high permeability sandstone, and injection was done without fracturing the reservoir. The model uses cumulative injected volume as the variable instead of pore volumes injected which similar models are based on. An alternative way of determining the filtration coefficient is chosen because results from laboratory tests are unavailable

The model gives a good correlation with field data from Grane, and realistic value are back calculated using the model with some uncertainty. The alternative way of determining the filtration coefficient gives a low estimate, and indicates that laboratory experiments should be done in order to test the model further.

Acknowledgement

This master thesis was carried out at University of Stavanger, in the department of Petroleum Engineering.

I would like to express my gratitude to all my fellow students who have made these five years in Stavanger a great experience

A special thanks to my supervisor, Jan Aage Aasen, for always having an open door for advice and support when needed

Table of contents

List of figures

List of tables

Abbreviations

BHP = Bottom Hole Pressure

BTEX = Acronym for Benzen, Toluene, Ethylbenzene and Xylen

CIV = Cumulative Injected Volume

DOWS = Downhole Oil/Water Separation

DREAM = Dosage related Risk and Effect Assessment

EIF = Environmental Impact Factor

FE = Flow Efficiency

FPSO = Floating Production, Storage and Offloading vessel

GOC = Gas Oil Contact

NORM = Naturally Occurring Radioactive Materials

OIW = Oil In Water

OLF = Norwegian Oil Industry Association

OWC = Oil Water Contact

PVI = Pore Volumes Injected

PAH = Polycyclic Aromatic Hydrocarbons

PEC = Predicted Environmental Concentration

PNEC = Predicted No Effect Concentration

PW = Produced Water

PWRI = Produced Water Re-Injection

SPE = Society of Petroleum Engineers

SPIN = Simulates and Predicts the Injectivity

SUBSIS = SUBsea Separation, Injection System

TSS = Total Suspended Solids

WQR = Water Quality Ratio

Table of symbols

A = area for porous media fluid is injected into

a = constant

A_H = Hamaker constant

A_s = porosity dependent parameter

b = constant

C = solids concentration in injected water

C_0 = initial solids concentration in injected water

C_D = dimensionless solids concentration in injected water

C_{oil} = oil concentration in injected water

μ = viscosity of fluid

d_g = grain diameter

d_p = particle diameter

e = electric charge of an electron

$E(\lambda r_w)$ = error function

f = Coulomb frictional coefficient

F_B = buoyancy force

F_D = drag force

F_e = electrostatic force

F_f = frictional force

F_G = gravity force

F_L = lift force

F_v = Van der Waals attraction force

g = gravitational constant

h = height

h_c = filter cake thickness

h_m = length of completion interval

h_r = reservoir height

II = injectivity index

II_0 = initial injectivity index

J = Impedance

J_{BL} = impedance during particle free saltwater injection

k = reservoir permeability

k_0 = initial reservoir permeability

k_b = Boltzmann's constant

k_c = filter cake permeability

k_d = damaged zone permeability

k_h = horizontal permeability

k_{rowi} = relative permeability for oil at the presence of water

k_{rwor} = relative permeability for water at the presence of residual oil

k_v = vertical permeability

L = length of core/formation damage

m = slope during internal filtration

m_c = slope during external filtration

m_ω = slope during internal filtration using intermediate pressure point

n_i^0 = number of ions per unit volume in the fluid

P = pressure

P_D = dimensionless pressure

P_r = reservoir pressure

P_w = wellbore pressure

q = injection rate

r = radius

R = variable describing correlation between data points

R_C = half distance between injector and producer

r_d = damage zone radius

R_D = shortest distance between two neighbouring particles

r_D= dimensionless radius

r_e = effective injection radius

Re = Reynolds number

r_p= radius of particle

r_w = wellbore radius

S = Skin factor

S_a = anisotropy skin

S_c = completion skin

S_m = mechanical skin

S_t = total skin

T = temperature

t = time

t_D = dimensionless time (pore volumes injected)

t_{Dtr} = dimensionless transitional time

t_{tr} = transitional time

U = fluid velocity

U_f = filtrate velocity

U_p = particle velocity

V = cumulative injected volume

V_{tr} = transitional cumulative injected volume

w_i = empirical variable

x = physical variable

x_i = empirical variable

X_w = dimensionless well coordinate

y = physical variable

y_i = empirical variable

z_i = empirical variable

z_i^2 = number of valence electrons per unit volume in the fluid

α = critical porosity fraction

β = formation damage coefficient

γ = porosity dependent parameter

ε_0 = permittivity of free space

ε_r = dielectric constant of fluid

ζ= zetta potential

κ= thickness of the double layer bond

η = total collection efficiency

η_D = collection efficiency due to diffusion

η_E = collection efficiency due to Electrostatic forces

η_{Im} = collection efficiency due to impaction

η_{In} = collection efficiency due to interception

η_s = collection efficiency due to sedimentation

θ = angle between grains

θ_a = hole angle

λ = filtration coefficient

λ_0 = initial filtration coefficient

ρ_f = fluid density

ρ_o = oil density

ρ_p = particle density

ρ_w= water density

σ = deposited particle concentration

σ_m = maximum deposited particle concentration

σ_y = standard deviation

τ_w = shear force

ϕ = porosity

ϕ_0 = initial porosity

ϕ_c = filter cake porosity

ψ_S = stern potential

ω = intermediate pressure point position

1 Introduction

1.1 Motivation

Mechanisms behind injectivity decline are not fully understood, and the models currently available are based on empirical values in addition to properties of the reservoir and fluid. This gives a good correlation, but the ultimate goal should be to express the injectivity decline without using empirical values. The solids that are in the produced water will have different sizes, and this can be represented in a size distribution.

Theory suggests that the mechanism behind particle deposition do not follow a linear trend, but rather an exponential trend. This can be seen in the model proposed by Happel (1958). This indicates that the particle distribution should also be included into the model, and not only an average particle diameter (Happel, 1958).

The models for injectivity decline available today uses cumulative injected pore volume, where the area of the formation is included into this parameter. The effect of increasing the length of the injection interval and by that increasing the area is not easy to directly observe from these models.

1.2 Objectives

The objectives of this thesis are to give a better understanding of challenges with produced water management with a special focus on produced water re-injection. The focus of this thesis will be on mechanism behind internal and external filtration leading to injectivity decline and creating a model based on previous models, but by using cumulative injected volume as a variable. The objectives of the thesis can be seen in the bullet points below:

- Give a holistic view of challenges with produced water management and different solutions, with focus on produced water re-injection.
- Describe the different forces that are acting on a particle in fluid flowing through porous media and the different mechanisms that leads to particle deposition.
- Create a model that describes the effect of internal and external filtration based on previous models, but use cumulative injected volume as a variable.

- Use the theory behind particle capturing to calculate the filtration coefficient, and including the particle distribution rather than the average value.
- Test the model based on data available for Grane well G-32, and discuss if the back calculated values for formation damage coefficient, filter cake porosity and permeability are realistic values.
- Discuss strengths and weaknesses in the created model.

1.3 Approach and Organization

This thesis is based on models created by authors like Sharma, Khatib, Wennberg and Bedrikovetsky, and modified using a different approach from the same equations. All simulations have been done in Microsoft Excel.

The thesis has the following configuration:

- Chapter 2 provides general information about produced water, contaminations in produced water, produced water management methods and methods to remove contaminations from the produced water.
- Chapter 3 describes different forces acting on a particle in a fluid flowing in a porous media.
- Chapter 4 describes the different mechanisms leading to particle deposition in a porous media and how these mechanisms can be related to the filtration coefficient.
- Chapter 5 gives information about a model for injectivity decline provided by Pavel Bedrikovetsky (2007).
- Chapter 6 derives a simple model created on the same standpoint as previous models, but uses some alterations.
- Chapter 7 discuss the model derived in chapter 6 and recommendations for further work.

(Da Silva, Bedrikovetsky, Van den Broek, Siqueira, & Serra, 2004; Khatib, 1994; Pang & Sharma, 1997; Wennberg & Sharma, 1997)

2 Produced water

Most petroleum reservoirs have formation water beneath the hydrocarbon bearing zones. This formation water can be either seawater or freshwater, and have been trapped for millions of years in a porous reservoir rock beneath layers of impermeable rocks. This water will be produced alongside hydrocarbons in varying amounts. In the early phase of production, it can be in small amounts as the water is usually condensed and in an oil/water emulsion. Water may also be produced in a free liquid phase later in production. The free water phase comes from underlying free water zones that have coned upwards due to lower viscosity in water.

The global average of produced water is today around 75% of the well stream, with some cases as high as 98%. These high amount of water produced along with the hydrocarbons makes water disposal system a very important factor when designing the offshore structure. The produced water must be handled in a cost efficient way and according to local legislations. This can be a challenge as the legislations regarding produced water disposal are gradually becoming stricter (Lee, Neff, & DeBlois, 2011).

1.1 Composition of produced water

Produced water consists of a complex mixture of organic and inorganic chemicals. The properties of produced water depend on the environment the water has been in, and will vary from field to field. These factors can be depth, geological age, chemical composition of the hydrocarbons, chemistry of the rocks and polymers used to enhance reservoir properties (Lee et al., 2011).

1.1.1 Salinity of produced water

Produced water usually have a greater salinity than seawater, and salinity usually increase slightly with depth. Density of the produced water will also increase with increasing salinity. Below you can see a table with typical concentration of elements in produced water and in seawater (Lee et al., 2011).

Element/Ion	Seawater	Produced water	
		Highest concentration observed (mg/kg)	Range of mean concentrations (mg/kg)
Salinity	35,000		5,000-300,000
Sodium	10,760	120,000	23,000-57,300
Chloride	19,353	270,000	46,100-141,000
Calcium	416	205,000	2,530-25,800
Magnesium	1,294	26,000	530-4,300
Potassium	387	11,600	130-3,100
Sulfate	2,712	8,400	210-1,170
Bromide	87	6,000	46-1,200
Strontium	0,008	4,500	7-1,000
Ammonium	0	3,300	23-300
Bicarbonate	142	3,600	77-560
Iodide	167	1,410	3-210
Boron	4.45	450	8-40
Carbonate	0	450	30-450
Lithium	0.17	400	3-50

Table 2.1 Concentration of the most common elements in produced water compared to seawater (Collins, 1975)

We observe that the concentration of different elements/ions vary greatly between seawater and produced water, and that produced water generally have higher concentrations of the different elements/ions. These higher concentrations increase the toxicity of produced water. Sulphur and sulphate content can also be a problem in re-injection wells because of scale formation (Pillard, Tietge, & Evans, 1996).

1.1.2 Organic content in produced water

There are several different types of naturally occurring organic chemicals in produced water, and below you can see a table of the most common classes:

Chemical class	Concentration range (mg/L)
Total organic carbon	0.1-11,000
Total organic acids	0.001-10,000
Total benzene, toluene, ethylbenzene and xylenes	0.068-578
Ketones	1.0-2.0
Total Phenols	0.4-23

Table 2.2 Organic content in produced water (Neff, 2002)

2.1.1 Petroleum hydrocarbons

Petroleum hydrocarbons can be defined as organic chemicals consisting of only carbon and hydrogen. These are the chemical compounds of produced water with the largest environmental impact. The solubility of petroleum hydrocarbons decreases as the molecular weight increases. There are also two different groups of petroleum hydrocarbons: aromatic hydrocarbons and saturated hydrocarbons. The aromatic hydrocarbons have higher solubility in water than saturated at the same molecular weight.

Hydrocarbons that exist in produces water can either be dissolved in the water or be dispersed as oil droplets. Current separation techniques are quite efficient at removing dispersed oil, but dissolved oil is harder to remove along with metals, phenols and organic acids (Faksness, Grini, & Daling, 2004).

BTEX is an acronym for benzene, toluene, ethylbenzene, and xylenes. These are the most abundant hydrocarbons in produced water. Of these benzene is the most abundant. BTEX are volatile, and most of them are leaving the water phase and entering the gas phase during treatments (Terrens & Tait, 1994).

Polycyclic Aromatic Hydrocarbons (PAH) are hydrocarbons consisting of two or more aromatic rings fused together. PAHs have high toxicity in marine environments. The concentrations of PAHs can vary from 0,04 mg/L to 3,0 mg/L before treatment. The PAHs in produced water primarily consist of water-soluble groups. Examples are naphthalene and phenanthrene. PAHs with higher molecular weight can be found in oil droplets in produced water, but is rarely found in properly treated produced water (Neff, 1987).

Increased amount of Oil In Water (OIW) have been found to decrease the injectivity. The effect of OIW on injectivity is not fully understood, but oil can be coating particles and effectively increasing their size and increasing the risk of particles sticking together. The injectivity decline due to oil might depend on the density and viscosity of the oil.

2.1.2 Metals

Produced water can contain substantially higher concentration of metals than seawater. The concentration varies based on the properties and geological age of the formation. Table 2.3 shows concentration ranges in parts per billion (ppb) of different metals from 12 different platforms in the North Sea (Collins, 1975).

Metal	Seawater (ppb)	Produced water in North Sea (ppb)
Arsenic	1-3	90
Barium	3-34	13,500
Cadmium	0.001-0.1	<10
Chromium	0-1-0.55	1-10
Copper	0.03-0.35	137
Iron	0.008-2.0	12,000-28,000
Lead	0.001-0.1	0.1-45
Manganese	0.03-1.0	1,300-2,300
Mercury	0.00007-0.006	<10
Nickel	0.1-1.0	0.1-420
Zinc	0.006-0.12	10-26,000

Table 2.3 Metals in produced water (Neff, 2002)

Iron, barium, manganese and zinc have a significantly higher concentration in produced water than in seawater. Part of the reason is that free oxygen is not present at reservoir conditions, and cannot react with the metals. When these dissolved metals are exposed to oxygen in the atmosphere the metals precipitates (Neff, 1987).

2.1.3 Radioactive isotopes

There are several radioactive isotopes present in the reservoir, and some of these gets dissolved in the water that is later produced. The most common Naturally Occurring Radioactive Materials (NORM) present in produced water are radium-226 and radium-228. These isotopes are radioactive decay derived from uranium-238 and thorium-232 (Kraemer & Reid, 1984; Reid, 1983).

2.1.4 Production chemicals

Chemicals that are injected into the reservoir in some way will also affect the water present and later produced. Chemicals have very many uses and some are used as additives to prevent gas hydrates, scales and corrosion. Polymers can also be used to improve recovery by polymer flooding the reservoir during water injection or by acidizing the reservoir for higher flowrate. Some chemicals will remain in the oil phase as they are more solute in oil, while others will remain in the produce water as they are water-soluble. Some of these chemicals can be toxic like biocide or corrosion inhibitors, and can give environmental issues (Lee et al., 2011).

2.2 Particles from the well

Metal debris from the casing will be present in the produced water due to erosion of the casing, and can increase the particle concentration. Most of the metal particles will be rust particles, as they will be released from the casing during injection.

Plugging due to particles that are picked up after the separation process is usually not considered in the plugging models as the amount of these particles are unknown. Factors like the type of well completion, injection casing grade and length of the well will also affect the number of particles from the well

2.3 Regulation of produced water discharge in Norway

There are different legislations for different parts of the world. Regulations for produced water discharge in areas controlled by Norway will be discussed in this section. Zero impact on the environment is the ultimate goal for produced water management solutions in areas controlled by Norway (Green, 2016).

From the pollution control act by the Norwegian environment agency we have:

- "Efforts shall be made to prevent any occurrence or increase of pollution, and to limit any pollution that does occur (§2, no. 1)"
- "Efforts to avoid and limit pollution and waste problems shall be based on the technology that will give the best results in the light of an overall evaluation of current and future use of the environment and economic considerations (§2 no. 3)"
- "No person may possess, do, or initiate anything that may entail a risk of pollution unless this is lawful pursuant to section 8 or 9 or permitted by a decision made pursuant to section 11 (§7)"
- "The pollution control authority may on application issue a permit for any activity that may lead to pollution (§11)"

This gives general information about how waste shall be handled on the Norwegian Continental Shelf, and does not only focus on produced waters. Regulations specific for Produced water is listed below (§60):

- "OIW as low as possible and max 30 ppm"
- "Duty to perform risk assessments of discharges of PW and to update them when significant changes in the discharge or minimum every 5 years (risk based approach)"
- "Duty to establish and maintain a best practice for operation and maintenance of the processing plant, comprising treatment units incorporated in the plant on the individual facility"
- "Duty to regularly consider possible technical solutions that can reduce the environmental impact of discharge of PW (risk based approach)"

What we see from these regulations is that there is only one specific requirement and that is that OIW should be as low as possible and maximum 30 ppm. The other requirements are more diffuse and must be assed in each case. One of the ways to determine the environmental impact is by using the Environmental Impact Factor (EIF) (Green, 2016).

The Norwegian Oil Industry Association (OLF) wanted to quantify the environmental benefits of different solutions and developed EIF. EIF is based on hazard assessment and environmental risk of produced water discharges, and takes into consideration both the composition and the amount of the discharge. The EIF calculated on a platform can then be used to find the best available technologies for produced water discharge in a cost efficient way. Lower value of EIF means lower impact on the environment. The EIF is often calculated by a Dosage related Risk and Effect Assessment Model (DREAM) on both a local and global scale, where a global scale is the Norwegian continental Shelf. The DREAM model is usually based on Predicted Environmental Concentration (PEC) and Predicted No Effect Concentration (PNEC) (Green, 2016; Johnsen, Frost, Hjelsvold, & Utvik, 2000).

The regulations for produced water discharge changes over time towards a zero impact regulation. This gives uncertainty when designing a system for produced water management, and an alternative solution to discharge can be economically viable. Produced water re-injection is a method that follows the zero impact philosophy as there is no discharge of contaminant water into the sea as long as no leakage occur.

2.4 Produced water disposal methods

Produced water is by volume the largest waste product within the oil and gas sector, and represent a significant cost for the industry. Khatib and Verbeek (2003) estimated that 76 billion barrels of water was produced yearly, and is around three times higher than the global oil production. It is estimated that in US there is produced 7 times as much water as oil, due to the amount of mature fields. It is worth mentioning that some of the produced water mentioned here also is from natural gas wells. These large volumes must be handled correctly according to local regulations. This section will be used to discuss options available for produced water management. The different methods to manage produced water is listed below:

- Discharge to sea
- Evaporation
- Re-injection

(Khatib & Verbeek, 2003; Neff, Lee, & DeBlois, 2011)

More companies are putting more focus on how to manage produced water cost efficient, and Shell has a program called “Water to value”. The purpose of this program is to minimize water production, reduce the cost of water treatment and have existing facilities handle larger amounts of produced water.

A mixture of oil, gas, water and solids will during production travel through the wellbore to the surface. The first stage is to separate these from one other. Segregation of the different phases are usually accomplished by a gravity separator. It uses the principle that the different phases have different density where the gas float on top of the oil, the oil float on top of the water and the solids fall to the bottom. This only separated the free phases, and the water will contain some oil emulsions and vice versa, and some particles will be too small to separate by gravity in the time spent in the separator (Neff et al., 2011).

2.4.1 Discharge to sea

Discharge to sea is the option where the produced water is purified according to local regulations and then released into the sea. This option is the most used option for produced water management, but this may change due to changes in the regulations for discharge (Neff et al., 2011).

2.4.2 Evaporation

Evaporation is a method for onshore installations, and it is when water is transformed into water vapour. The rate of evaporation is dependent on the temperature, humidity and wind. The water is placed in a hole with large surface area, where the water will evaporate naturally and hydrocarbons will be left. Produced water will be removed if the evaporation rate is greater than the inflow rate. This method is more effective in dryer climate with higher average temperature. A problem with such installations is that the pool of water contains hydrocarbons, and is a potential hazard to animals. A net can be set up to prevent birds from landing there (Neff et al., 2011).

2.4.3 Re-injection

Re-injection is a water disposal method where the produced water is injected into a porous formation. This can be done in a producing formation and at the same time maintaining the reservoir pressure. All the produced water is not always needed for pressure support, and injecting into a non-production water bearing formation can be a solution. Formations chosen for re-injection typically exhibits high permeability, porosity and gives a good injectivity. A formation where injection is possible below the fracturing pressure is preferred. Operators wants to avoid formations with excessive faulting, vertical fractures, weak cap rock and improperly cemented wellbores. Formation used for re-injection must be geologically isolated from any drinking water sources, but this is usually only a concern for onshore re-injection. (Lee et al., 2011)

2.5 Produced water separation methods

There are several different methods that can be used to remove contaminations in the produced water. Different methods will be discussed in this section with a focus on offshore separation.

2.5.1 Downhole separators

Downhole Oil/Water Separation (DOWS) separators are used to separate oil and water at the bottom of the well, where the water is pumped directly into the formation. The oil rich well stream continue towards the surface. DOWS uses an oil/water separator with one or more pump. The separators currently used in DOWS have been hydro cyclones and gravity separation. All trials for DOWS have this far been conducted onshore except one well drilled in China, which failed after a couple of weeks due to a bolt not properly tightened. Several onshore wells also had problems with that the DOWS performed worse than expected, or stopped working after a few weeks/months of production. New installations of DOWS are very rare, even though there are examples of DOWS installations that are successful as well.

A larger flowrate of oil can be achieved by using DOWS due to less water in the tubing. A DOWS does not take up any place on a platform and reduces the need of surface separation. The DOWS does not give as good separation as the separators on the platform, and this result in more OIW and TSS been injected into the formation and injection under fracturing conditions are needed (Neff et al., 2011).

2.5.2 Seabed separators

Seabed separators separated oil for water on the seabed, and reduce the amount of water sent to the platform. This reduces the need of submersible pumps to lift the fluid column to the platform, and the separator does not take any place or weight on the platform. There is also more space available on the seafloor than downhole, and easier to do maintenance on compared to a DOWS.

Fluids from one or more well are sent to a seabed separator for separation, where the water is sent for re-injection and the oil is sent to a platform or a Floating Production, Storage and Offloading vessel (FPSO). The company ABB developed a SUBsea Separation and Injection System (SUBSIS) at the Troll field in Norway (2001). The SUBIS module is 17 m long and wide, 6 m high, and weighs 400 tons. The SUBSIS handled a maximum of 60,000 bbl/d, but had a typical flow of 20,000 bbl/d. The initial oil concentration in the water after separation was at 600 ppm, but fell to 15 ppm. The troll platform was able to produce an extra 2.5 million bbl during the trial year, because water was separated at the seabed and did not occupy the water handling equipment. A similar seabed separator was installed on the Tordis field in 2007, and the separator is expected to extend the life of the Tordis field by 15-17 years. Seabed separators are however a costly investment, and the technology is relatively new and does have a high risks involved (Neff et al., 2011; Von Flatern, 2003; Wolff, 2000).

2.5.3 Physical separation

Physical separation uses separation that is based on gravity, centrifugal forces or bridging and straining of particles. Most of the free oil and some of the dispersed oil can be separated using physical separation, but very little of the oil that is dissolved in the water is removed.
Different physical separation methods are listed below:

- Advanced separators
- Hydrocyclones
- Filters
- Centrifuges

(Neff et al., 2011)

2.5.3.1 Advanced separators

Oil with lower specific gravity than water will rise. The rise velocity of these oil droplets will depend on diameter, viscosity, velocity of water and the difference in density between oil and water. Smaller oil droplets will be left in the water phase if insufficient time is spent in the separator, as smaller droplets will rise more slowly. Advanced separators contain an internal structure that gives the smaller droplets higher chance of reaching the oil water contact in the separator before the water reach the end of the separator (Neff et al., 2011).

2.5.3.2 Hydrocyclones

Hydrocyclones apply a centrifugal force to separate different substances with different densities. Hydrocyclones can use liquid/solids separation or liquid/liquid separation. Oil is usually separated from the water in produced water using a liquid/liquid separator. Produced water containing oil is sent into the hydrocyclone where the heavier water will spin closer to the outside and the oil is in the middle. The lighter oil is eventually forces upwards towards the upper outlet as the diameter of the hydrocyclone is reduced, while the water will move to the lower outlet (Neff et al., 2011).

2.5.3.3 Filtration

Filtration uses filters with a specific size of each pore, and particles in the fluid that are larger than the pore size will be blocked, while water and smaller particles flow through. The filters used offshore are usually a vessel containing grains of desired size and removes solids in the same way they get stuck during internal filtration. This is described further in section 4.3.

There exist different types of finer filters that are classified as membranes to remove finer particles as salt or inorganic chemicals. These membranes are categorized after pore size. The different categories from largest to smallest includes:

- Microfiltration
- Ultrafiltration
- Nanofiltration
- Reverse osmosis

The pore size range for each of the category can be seen in the table below:

	Microfiltration	Ultrafiltration	Nanofiltration	Reverse osmosis
Pore size	0.01-1.0 µm	0.001-0.01 µm	0.0001-0.001 µm	<0.0001 µm
Types of materials removed	Suspended solids, clay, bacteria, viruses	Suspended solids, proteins, viruses, colloidal silica, fats	Sugar, divalent anions	Metal cations, acids, aqueous salts, amino acids

Table 2.4 Different categories of filtration

It requires greater amount of energy the smaller the pore size of the membrane, and the risk of plugging the membrane increases as well. Filtration is usually run in stages with the finest membrane last (Neff et al., 2011).

2.5.3.4 Centrifuges

Centrifuges uses the same principle as hydrocyclones to remove oil and solids from water. Substances with different densities will be separated due to centrifugal forces. Centrifuges generate a much higher centrifugal force than a hydrocyclone, and are capable of removing particles and oil droplet of smaller sizes. Centrifuges used for produced water separation generally have a vertically positioned spinning axis. Centrifuges are used when a strict policy is needed for the amount of oil in water and total suspended solids, but comes at a greater cost than the use of a hydrocyclone (Neff et al., 2011).

2.5.4 Coalescence

The principle behind coalescence is that the oil droplets rise velocity will increase with increasing oil droplets diameter, and more oil will be removed by other technologies by making smaller oil droplets join together. Oil droplets are joined together on a surface typically of fiberglass, polyester, metal or Teflon® arranged in a mesh. Finer mesh is able to capture and coalesce smaller oil droplets, but are at the same time more prone to be filled by solids. Coalescence is a way to remove oil, and the mesh is not designed to remove solids. Solids should be removed before by another type of separator (Neff et al., 2011).

2.5.5 Flotation

Flotation inject bubbles of gas into the bottom of a tank with produced water. The bubbles will rise due to lower density and they will “pick up” oil droplets and particles and lift them to the top of the tank where they will be removed. Different technologies exist for gas injection where different bubble sizes are the main difference. Chemicals can also be added to break the emulsion or aid the flotation process (Neff et al., 2011).

2.5.6 Polymer extraction

Polymer extraction is a method to remove hydrocarbons from produced water by passing the water though a porous media packed with polymer beads containing a liquid that removes dissolved hydrocarbons and organics due to attraction forces between the liquid and hydrocarbons. This method can be used when a lower oil content than 5mg/L is desired (Neff et al., 2011).

3 Forces acting on a particle in a colloidal system

Several different forces are acting on particles as they move in a colloidal system before they are deposited. In this chapter these forces will be discussed to get a better understanding of how particles are transported and deposited. These forces are:

- Lift force
- Drag forces
- Buoyancy
- Brownian motion and diffusion
- Electrostatic forces
- Van der Waals attraction
- Friction force

3.1 Lift force

Shear flow will induce a lift force experienced by the particles. It can be explained by using Bernoulli's equation. Particles will slow down fluid right behind it, while the fluid that is ahead of the particle will have a higher speed. This gives rise to a velocity profile and a pressure differential according to Bernoulli's equation (3.1). Particles will experience a lift force from this pressure differential.

$$\frac{dP}{\rho_f} + 0.5U^2 + gh = constant \qquad \textit{Equation 3.1}$$

Where P is pressure, ρ_f is the density of the fluid, U is the velocity of the fluid, g is the gravitational constant and h is the height difference between the inlet and outlet. From experiments and theoretical analysis Rubin et al (1977) found that the lift force (F_L) can be expressed as:

$$F_L = 0.761 \frac{{\tau_w}^{1.5} {d_p}^{0.5}}{\mu} \qquad \textit{Equation 3.2}$$

Where τ_w is the shear force, d_p is the particle diameter and μ is the viscosity of the fluid. (Rubin, 1977).

3.2 Drag force

Drag forces are due to the fluid resistance, and is a force acting in the opposite direction to the relative motion. The resistance from the surrounding fluid is due to viscous shear forces when flowing around the particle. The drag force on a particle is dependent on the shape, size of the particle, fluid velocity, viscosity and density of the fluid.

The drag force will have two components when a particle has been deposited. One is parallel to the surface (tangential drag force) and the other is perpendicular (normal drag force). The normal drag force is due to the filtrate velocity that is creating lower pressure under the particle pushing it down (Farajzadeh, 2004).

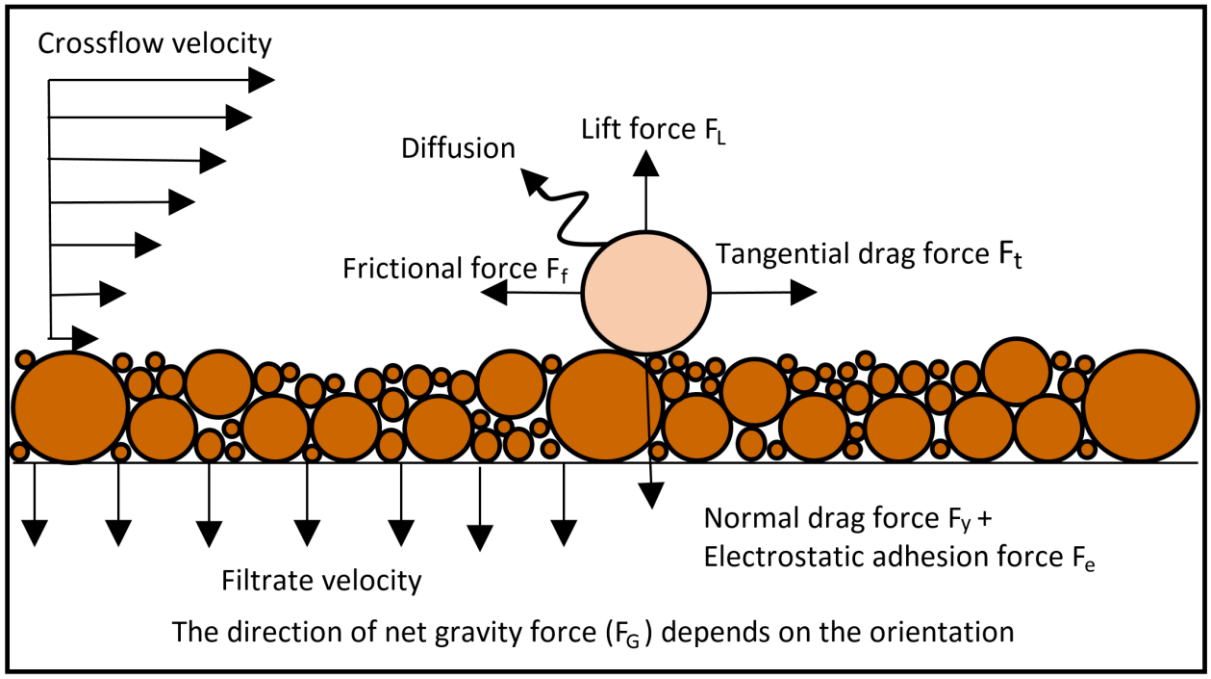

Figure 3.1: Forces acting on a particle in a colloid system

3.2.1 Flow over a sphere

Both the normal and the tangential drag contribute to the total drag on spherical particles. To accurately calculate the forces present in the system, we need to know what type of flow we have. To do this we can use the ratio between inertia forces and viscous forces, better known as the Reynolds number (Re) (Fox & McDonald, 1994).

$$Re = \frac{\frac{\rho V^2}{d_p}}{\frac{\mu V}{{d_p}^2}} = \frac{\rho V d_p}{\mu} \qquad \textit{Equation 3.3}$$

During produced water re-injection, we normally have grain diameters no larger than 40 µm and velocities up to 0.02 m/s when flowing into the reservoir. (If we assume we have a formation area of 75m^2 we are injecting water into and a porosity of 0.30, we need an injection rate of 38 900 m^3/ day to achieve a velocity of 0.02m/s). Using these values, we get:

$$Re = \frac{1003 * 0.02 * 40 * 10^{-6}}{10^{-3}} = 0.8$$

For Reynolds numbers lower than 1 we have what is called Stokes flow. The inertia forces in Stokes flow have been shown to be very small, and can be neglected. The drag force (F_D) on a spherical particle can then be calculated by:

$$F_D = 3\pi\mu d_p U_f \qquad \textit{Equation 3.4}$$

Where U_f is the filtrate velocity (Fox & McDonald, 1994).

3.3 Buoyancy

Buoyancy is due to the gravitational pull on the particle and the fluid, the difference in density between the particle and fluid will determine if the buoyancy act in a vertical downward direction or vertical upwards direction. To calculate the buoyancy force (F_B):

$$F_B = -\frac{1}{6}\pi {d_p}^3 g(\rho_p - \rho_w) \qquad \textit{Equation 3.5}$$

Where ρ_p and ρ_w are the particle and water density respectively.

3.4 Electrostatic forces

There is electrostatic repulsion between particles that prevents them to clump together. Colloid particles have a charge, and there is also a sea of ions in the fluid surrounding the particles, and the total sum of these ions should be the same and oppositely charge to maintain electric neutrality. These ions are attracted to the oppositely charged ions in the particle (Hunter, 2001).

All matter with temperature above zero Kelvin is subjected to thermal motion. This is a random motion of electrons, molecules, atoms or subatomic particles. This random motion will increase with higher temperatures. This is also the case for ions, and this thermal motion counteracts the attraction between ions and electrically charged particles. This results in the ions creating a double layer around the particle where the thermal motion is in equilibrium with the attraction between ions and particles. The inner layer is the surface charge, and consists of ions that are adsorbed onto the surface of an object due to chemical interactions. The second layer is made up of free ions creating a diffuse layer that are attracted to the first layer due to the coulomb force and effectively neutralizes the charge of the inner layer (Hunter, 2001).

The repulsive force between to particles with the same radius, where the radius of the particle is much greater than the thickness of the electric double layer, can be calculated by this equation proposed by Hunter (1987):

$$F_e = -2\pi\varepsilon_0\varepsilon_r r_p \kappa {\psi_S}^2 \frac{e^{-\kappa R_D}}{\ln(1-e^{-\kappa R_D})} \qquad \textit{Equation 3.6}$$

$$R = \left(\left[\frac{\pi}{3cos\theta(1-\varepsilon_0)}\right]^{\frac{1}{3}} - 1\right) d_p \qquad \textit{Equation 3.7}$$

Where ε_0 is the absolute permittivity of free space ($\varepsilon_0 = 8.85 * 10^{-12}\frac{C^2}{Jm}$), ε_r is the dielectric constant of the fluid (water: $\varepsilon_r = 78.5$), r is the radius of the two particles, R_D is the shortest distance between two neighbouring particles in a hexagonal packing structure, θ is the angle between grains. For a hexagonal structure we get that θ = 54.7° and ψ_S is the stern potential. The stern potential is often assumed to be equal to the zeta potential (ξ), which is the electric potential between the outer layer of the particle and the stationary layer of fluid attached to the particle. κ is the thickness of the double layer bond:

$$\kappa = \left[\frac{e^2 \sum n_i^0 z_i^2}{\varepsilon_0 \varepsilon_r k_b T}\right] \qquad \textit{Equation 3.8}$$

Where e is the electrical charge of an electron ($1.6*10^{-19}$C), z_i^2 and n_i^0 are the number of valence electrons per unit volume in the fluid and number of ions per unit volume in the fluid respectively. T is the absolute temperature given in Kelvin and k_b is the Boltzmann constant ($1.4*10^{-23}$ J/K) (Hunter, 1987).

3.5 Van der Waals forces

Van der Waals forces are weak attraction forces due to polarity between uncharged molecules. These forces must overcome the electrostatic forces for particles to clump together. These forces become significant for smaller particles. These forces are also only present for molecules of the same bonds. Van der Waals forces are sometimes also called London forces, and are different from hydrogen bonds, covalent bonds and ionic bonds (Hunter, 2001).

Van der Waals attraction forces are due to the constant movement of electrons that creates fluctuations of the charge distribution in atoms. This charge fluctuation gives rise to temporary polarity to an adjacent atom, and this polarity only last for a very short time before it disappears. The attractive forces between atoms are according to theory additive (Hunter, 2001).

To calculate the attraction force (F_v) we can use the formula proposed Hunter. Here it is assumed that the radius of the particle is much greater than the thickness of the electric double layer:

$$F_v = -\frac{A_H {d_p}^6}{6{R_D}^2(R_D + 2d_p)^2(R_D + d_p)^3} \quad \textit{Equation 3.9}$$

Where A_H is the Hamaker constant (J) (Hunter, 2001).

3.6 Brownian motion (diffusion)

The random motion due to bombardment of smaller particles is called brownian motion (or diffusion) after Robert Brown, who was a botanist who examined how pollen grains move. The same motion is observed with any small particle. Brownian motions occur when smaller water molecules collide with a particle and results in the particle moving in what seems random motion and is often called random walk. Belfort et al (1994) found that this motion has been found to be back transporting particles into filter media they just passed through (Batchelor, 1976; Belfort, Davis, & Zydney, 1994).

Trerrin and Doshi (1980) assumed that diffusion is the only mechanism back transporting particles and proposed an equation for the permeate flux in crossflow filtration. They found that the flux was depending on the viscosity, porosity, wall shear stress, filter length and the Brownian diffusion coefficient that is determined by Stokes-Einstein equation (Trettin & Doshi, 1980).

3.7 Friction force

Frictional force is a force that works in the opposite detection of the movement. Coulomb (1785) found that the frictional force is proportional to the sum of normal forces. In a colloid system this can be expressed as:

$$F_f = f(F_D + F_e + F_G) \qquad \textit{Equation 3.10}$$

Where f is the Coulomb frictional coefficient that is independent on velocity and contact area, F_f, F_D, F_e and F_G are the frictional, drag, electrostatic and gravity force respectively (Farajzadeh, 2004).

4 Filtration theory

This chapter gives an introduction to formation damage and filtration theory. The chapter starts by discussing the skin factor, and how it relates to the injectivity index. The formation damage can be divided into internal and external filtration, and this chapter will discuss theory behind and different mechanisms behind internal filtration.

The total collection efficiency is due to different capturing mechanisms. This parameter describes the probability of a particle retained when traveling through a given length inside the reservoir. This can be expressed as the collection efficiency, η:

$$\eta = \frac{Number\ of\ particles\ retained}{Number\ of\ particles\ entering} \qquad \textit{Equation 4.1}$$

4.1 Skin factor

Variation in permeability in the region close to the borehole can be expressed with help from a dimensionless skin factor (S). A positive skin factor represents reduction in permeability compared to an undamaged open hole well. Reduction in permeability can be due to a number of reasons, including drilling damage, hole angle and blocking of pores. A negative skin factor indicates higher permeability than an undamaged open hole. This can be achieved by perforations, acidizing or hydraulic fracturing (Bellarby, 2009). The skin factor can be expressed as:

$$S = \left(\frac{k}{k_d} - 1\right) \ln\left(\frac{r_d}{r_w}\right) \qquad \textit{Equation 4.2}$$

Where k is the reservoir permeability, k_d is the damaged permeability, r_d and r_w is the damaged zone (assumed circular) and wellbore radius respectively (Bellarby, 2009).

As produced water is injected into the reservoir, some particles contained within the produced water will block pore throats, and this will result in reduced injectivity. Injectivity index, J, is a measurement of the amount of water injected into the reservoir with a corresponding differential pressure between the bottom of the wellbore and the reservoir (Bellarby, 2009):

$$J = \frac{q}{\overline{\Delta P_r} - \Delta P_w} = \frac{\mu S_t}{2\pi k h_r} \qquad \text{Equation 4.3}$$

Where q is the flowrate, P_r is the reservoir pressure, P_w is the wellbore pressure, S_t is the total skin, μ is the viscosity, h_r is the height of the reservoir (Bellarby, 2009).

$$S_t = \frac{h_r}{h_m} F(S_m + S_a) + S_c \qquad \text{Equation 4.4}$$

Where h_m is the measured length of the completion interval. $S_m, S_a \; and \; S_c$ are the mechanical, anisotropy and completion skin respectively (Bellarby, 2009).

Anisotropy skin is the skin due to difference between horizontal and vertical permeability. The anisotropy skin can be expressed as:

$$S_a = \ln\left(\frac{2}{1+F}\right) \qquad \text{Equation 4.5}$$

$$F = \frac{1}{\sqrt{cos^2\theta + \frac{k_v}{k_h} sin^2\theta_a}} \qquad \text{Equation 4.6}$$

Where k_v and k_h is the vertical and horizontal permeability respectively and θ_a is the hole angle corrected for dipping formation. Horizontal permeability is generally much greater than vertical permeability and this gives a low value of $\frac{k_v}{k_h}$, and a high F in the case of a horizontal well. A high F will in result in a negative anisotropy skin factor. F is also multiplied with the mechanical skin and the anisotropy skin. This means that the mechanical skin is increased in formations with a high F and the anisotropy is decreased due to the anisotropy skin being negative. Horizontal wells give the possibility to have a longer completion section compared to a vertical well. The mechanical skin and anisotropy skin is also multiplied with h/h_m. This means that longer completion section will reduce the total skin (Bellarby, 2009).

Mechanical skin is observed when injecting produced water because of the particles and oil droplets. This usually result in a rapid injectivity decline as deposition of these particles will do severe damage to the formation, reducing the permeability (Bellarby, 2009). Lower injectivity means that a higher pressure is needed to inject the same amount of fluid. This increased pressure can result in unwanted fracture propagation. Cooling of the reservoir will affect the stresses in the rock, and increase this effect.

4.2 Formation damage

Damage done to the formation during re-injection is a function of several parameters. It is affected by the properties of the reservoir rock where the water is injected, the characteristics of the water and the amount of water injected during a time period. For a porous media the porosity and permeability are the most important parameters, and for produced water the amount of solids and oil present as well as the size distribution are the most important parameters.

There are several different problems than can lead to formation damage and reduced permeability, and one of the following scenarios may be applicable:

- Pure external filter cake build up
- Pure internal filtration
- Internal filtration initially and external filter cake build up after a transition time
- Internal filtration initially and simultaneous internal filtration and external filter cake built up after a transition time

There have been several attempts to quantify the damage done to the formation, and one of the earliest was Barkman and Davidson. They defined the time for the injectivity rate to fall to 50% of the initial injectivity as the injectivity half time. They also found four mechanisms for plugging: wellbore narrowing, invasion, perforation plugging, and wellbore plugging. They used an equation to predict the half time each of the four mechanisms as a function of the water quality ratio (WQR). WQR is defined as the ratio between the concentration of solids in the produced water to the permeability of the filter cake formed. The WQR was measured in a laboratory using core samples under constant pressure drop. The filtration volume is linear when plotted against the square root of time. Barkman and Davidsons equations were only valid for constant pressure (Barkman & Davidson, 1972; Farajzadeh, 2004).

The injection pressure in real wells will vary, and Hofsaess and Kleinitz (2003) introduced new equations to calculate the WQR. They defined the injectivity decline based on accumulated volume and could now vary the pressure (Hofsaess & Kleinitz, 2003).

Today injectivity decline is usually based on deep bed filtration theory using laboratory experiments to obtain a filtration coefficient and damage coefficient to model injectivity decline. Flow containing different particles through porous media has undergone a lot of researched, but the process is still not fully understood due to the complexity of such systems.

4.3 Internal filtration

The process where particles are retained inside the porous media is called internal filtration or deep bed filtration (Herzig, Leclerc, & Goff, 1970). Particles can be solids, dispersed oil or a colloidal system containing several smaller components acting as a single particle. In a flow containing particles some of these will settle down at different retention sites. These retention sites are natural deposition sites for particles inside the porous media. Listed below are the different retention sites. They are also illustrated in *Figure 4.1* (Farajzadeh, 2004).

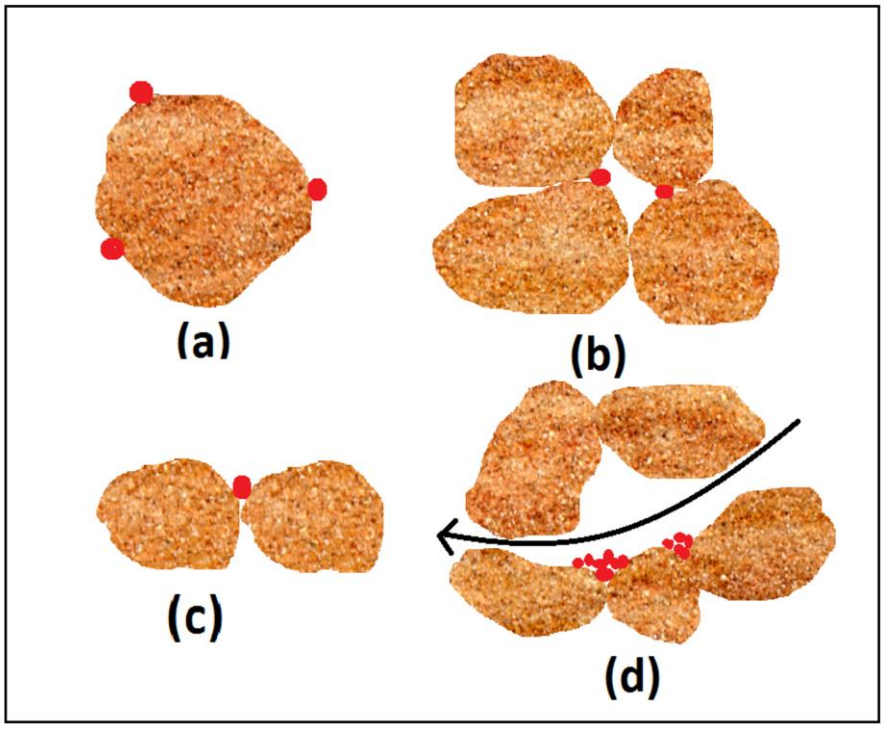

Figure 4.1 Types of retention sites: (a) surface site, (b) crevice site, (c) constriction site, (d) cavern site

- Surface sites:
  Particles are deposited on the surface of the grain because the particles are too large to penetrate the medium.
- Crevice sites:
  Particles get stuck at convex surfaces. These convex surfaces are typical for well-ordered grains.
- Construction sites:
  Particles are deposited in pore throats that are smaller than the diameter of the particle
- Cavern sites:
  Particles can be deposited in places where the flow velocity is no longer sufficient to keep the particles in the flow. These cavern sites are sheltered from the flow. (Farajzadeh, 2004)

4.3.1 Interception

Interception is when a particle following the fluid flow collides with the surface of a grain and is attached to it. Happel (1958) created a model for calculating the probability of particles hitting the grain surfaces for particles with the same density as the fluid:

$$\eta_{In} = \frac{3}{2} A_s \frac{{d_p}^2}{{d_g}^2} \qquad \textit{Equation 4.7}$$

$$A_s = \frac{2(1-\gamma^5)}{2-3\gamma+3\gamma^5-2\gamma^6} \qquad \textit{Equation 4.8}$$

$$\gamma = \sqrt[3]{1-\phi} \qquad \textit{Equation 4.9}$$

Where η_{In} is the collection efficiency due to interception, A_s and γ are porosity dependent parameters, d_p and d_g is the diameter of the particle and grain respectively and ϕ is the porosity (Farajzadeh, 2004; Happel, 1958).

4.3.2 Impaction

The density of solid particles will usually have a higher density that that of the fluid. When this is the case, the particles will experience inertia forces that will deviate the particles and results in particles attaching to a grain. The collection efficiency due to impaction:

$$\eta_{Im} = \frac{(\rho_p - \rho_f){d_p}^2 U_p}{18\mu d_g} \qquad \textit{Equation 4.10}$$

Where ρ_p and ρ_f are the density of the particle and fluid respectively, U_p is the particle velocity and μ is the viscosity of the fluid. We observe that the collection efficiency due to impaction is a function of the difference in particle and fluid density as well as the inertia. The effect of impaction will increase with higher density differences (Farajzadeh, 2004).

4.3.3 Sedimentation

If the density of the particle and fluid is different, so will the velocity be. This difference in velocity will result in the particle deviating from the fluid stream due to gravity and settle on grain surfaces. This is different from impaction in the sense that sedimentation is only an effect due to gravity, while impaction is the effect of inertia experienced by the particles when the fluid stream is changing direction. The collection efficiency due to sedimentation, η_s, can be expressed as:

$$\eta_s = \frac{(\rho_p - \rho_f){d_p}^2 g}{18\mu U_f} \qquad \textit{Equation 4.11}$$

Where g is the gravitational constant and U_f is the fluid velocity (Farajzadeh, 2004).

4.3.4 Diffusion

Random Brownian motion (diffusion) affects the movements of bigger grains due to collection with smaller grains/molecules. Brownian motion is discussed in more detail in section 3.6. Diffusion is only important for small particles (d_p<1µm), and can be neglected for bigger particles. The diffusion collection efficiency, η_D, can be expressed as:

$$\eta_D = 0.9\left(\frac{k_b T}{\mu d_p d_g U_f}\right)^{\frac{2}{3}} \qquad \textit{Equation 4.12}$$

Where k is the Boltzmann's constant ($1.380\ 6505 \times 10^{-23}$ J/K) and T is the absolute temperature in Kelvin (Farajzadeh, 2004).

4.3.5 Straining

Particles that are too small to pass through a pore throat will get stuck and prevent smaller particles to get through. The most important factor during straining is the ratio between the throat diameters and the particle diameter.

When particles get stuck due to a previous retained particle, we refer to it as bridging. It is also possible to get bridging when two or more particles tries to get through a pore throat at the same time. This is illustrated in Figure 4.2:

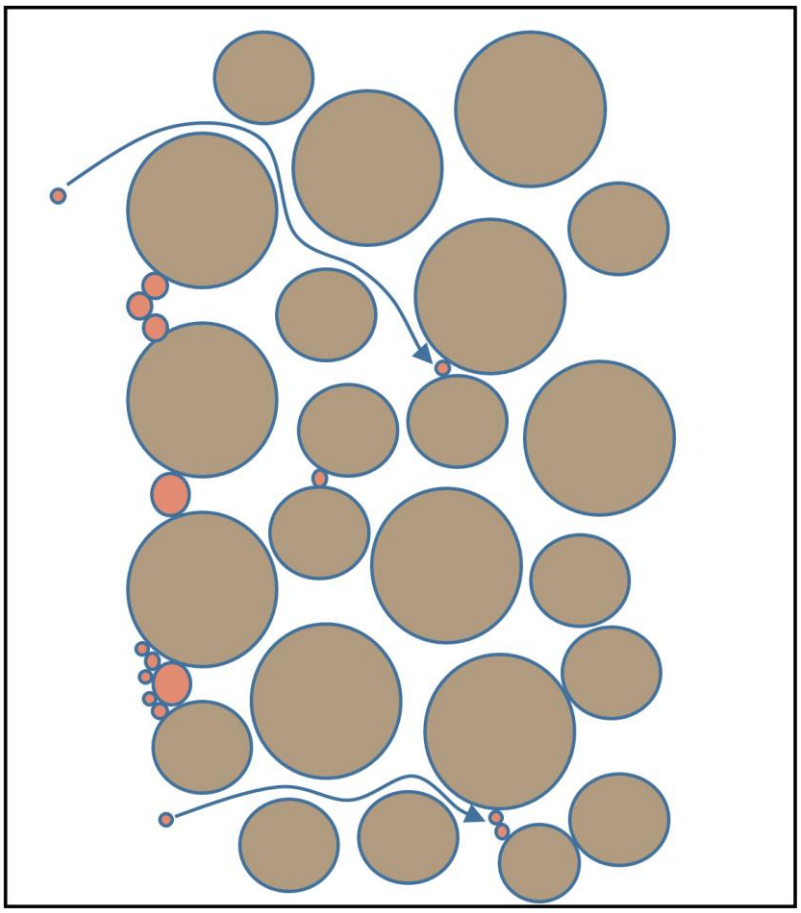

Figure 4.2 Illustration of how straining and bridging of particles occur

4.3.6 Electrostatic forces

For a particle that have landed on a grain to get stuck, there must be a greater force keeping the particle there as there is hydrodynamic forces present that can pick up the particles again. Electrostatic forces like Van der Waals attraction and double layer repulsion affect if a particle will attach to a grain.

Rajagopalan (1997) proposed an equation to calculate the collection efficiency due to electrostatic forces:

$$\eta_E = A_s \left(\frac{4A_H}{9\pi\mu}\right)^{\frac{1}{8}} \left(\frac{{d_p}^{\frac{13}{8}}}{(\varphi U_p)^{\frac{1}{8}} {d_g}^{\frac{15}{8}}}\right) \quad \textit{Equation 4.13}$$

Where A_H is the Hamaker constant (10^{-20}J). The total collection efficiency can be calculated by:

$$\eta = \eta_E + \eta_S + \eta_{In} + \eta_{Im} + \eta_D \quad \textit{Equation 4.14}$$

(Hiemenz & Rajagopalan, 1997)

4.4 Filtration and formation damage coefficient

The filtration coefficient (λ) is a dynamic quantity that describes the rate of particle deposition per unit length, and it changes with the number of previously deposited particles. There are different ways of determining the filtration coefficient that are based of theoretical and experimental work (Bedrikovetsky, Vaz, Furtado, & Serra de Souza, 2011).

The formation damage coefficient (β) shows how the permeability is reduced due to particle deposition inside the porous media. β is determined from measuring the pressure profile (Bedrikovetsky et al., 2002).

4.4.1 Happel's cell

Computer simulations have been carried out to determine the filtration coefficient for a pre-determined volume. Two different classes of computer simulations exist. "Flow through" models and "Flow over" models. "Flow over" models are models where the porous media is defined as several collectors, which the injected fluid containing particles flows over (Wennberg & Sharma, 1997).

Happel (1958) introduced a model for a Happel cell, which is a flow over model that contains spherical grains with a liquid shell around it. This is a simplified pore space, and does not take into consideration complex pore spaces as seen in a porous rock, but is a way to calculate the filtration coefficient without laboratory experiments. To calculate the initial filtration coefficient (λ_0):

$$\lambda_0 = \frac{3\eta(1-\phi)^{\frac{1}{3}}}{2d_g} \qquad \textit{Equation 4.15}$$

The collection efficiency (η) is calculated by Equation 4.14 (Happel, 1958).

4.4.2 Three-point pressure method

The traditional way of determining the filtration coefficient is by core flooding using produced water and measure the particle concentration before and after the core flood. Measuring the particle concentration is a difficult process and requires expensive equipment. Determining the formation damage coefficient, β, is determined from inexpensive pressure-drop measurements in the core. This section is based on the paper "Damage characterization of deep bed filtration from pressure measurements" (Bedrikovetsky et al., 2002).

The three-point pressure method is a way of determining the filtration and formation damage coefficient from pressure measurements at the core ends as well as at an intermediate point of the core. The problem with only taking pressure points from the two ends of the core is that only a combination of these two parameters can be found, or ranges for each of the two parameters.

We can get the injectivity of this core by measuring pressure at the two ends and the volumes injected. We get the slope m_c by using the least square method (described in A. Appendix) to draw a straight line between the points. We here want the injectivity during internal filtration, and may have to exclude later points where the filter cake has formed.

We already know the original injectivity, viscosity of the fluid, amounts of particles in the injection fluid, area we are injecting fluid through. The original permeability was measured before core flooding. We have this formula derived in chapter 6 that relates the slope (m) during internal filtration with the filtration and formation damage coefficient:

$$m = \frac{II_0 \beta \mu C_0 (1 - e^{-\lambda L})}{A^2 k_0} \qquad \textit{Equation 4.16}$$

Where II_0 is the initial injectivity, C_0 is the solids concentration, L is the length of the core, A is the formation area the produced water is injected into and k_0 is the initial reservoir permeability.

We observe that we now have one equation and two variables (λ and β). From this we can have relationship between them. We know all the other variables and can plot the formation damage coefficient as a variable of the filtration. The curve we see below is based on data from Grane well G-32, but should look similar with other data as well (Bedrikovetsky et al., 2002).

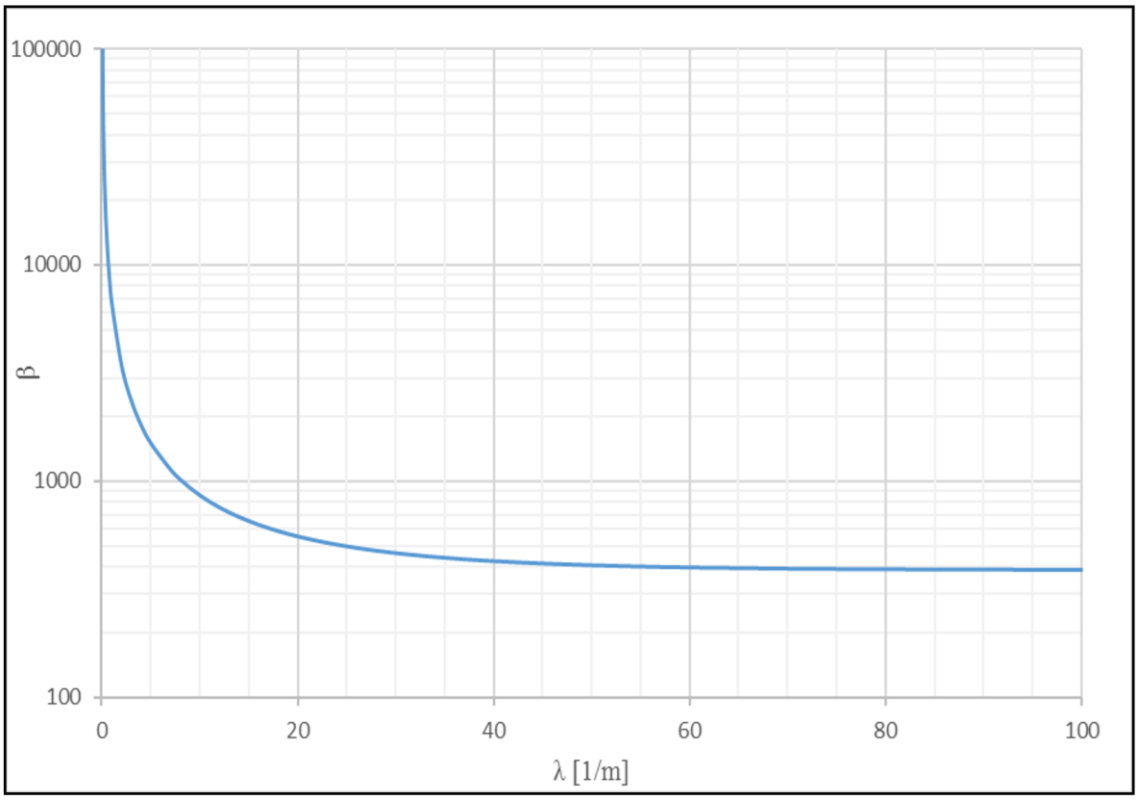

Figure 4.3 Formation damage coefficient as function of filtration coefficient

From Figure 4.3 we see that β and λ compensate each other. A low λ gives a high value of β, and as λ goes towards infinity the term $e^{-\lambda L}$ goes towards zero and β goes towards a specific value. The filtration coefficient can be determined by measuring the particle concentration at the end of the core, and then use this graph to determine the formation damage coefficient.

Both variables can also be determined by using a third pressure point. The internal damage inside the core is not evenly distributed, and higher damage will be observed closer to the

injection point. By using a third pressure point we get a second injectivity curve from the pressure drop in a part of the core. We can then obtain the slope m_ω. This slope will have a different value than the slope of the entire core due to unevenly distributed retained particles (Bedrikovetsky et al., 2002). An illustration of how the three-point pressure method is performed is presented below:

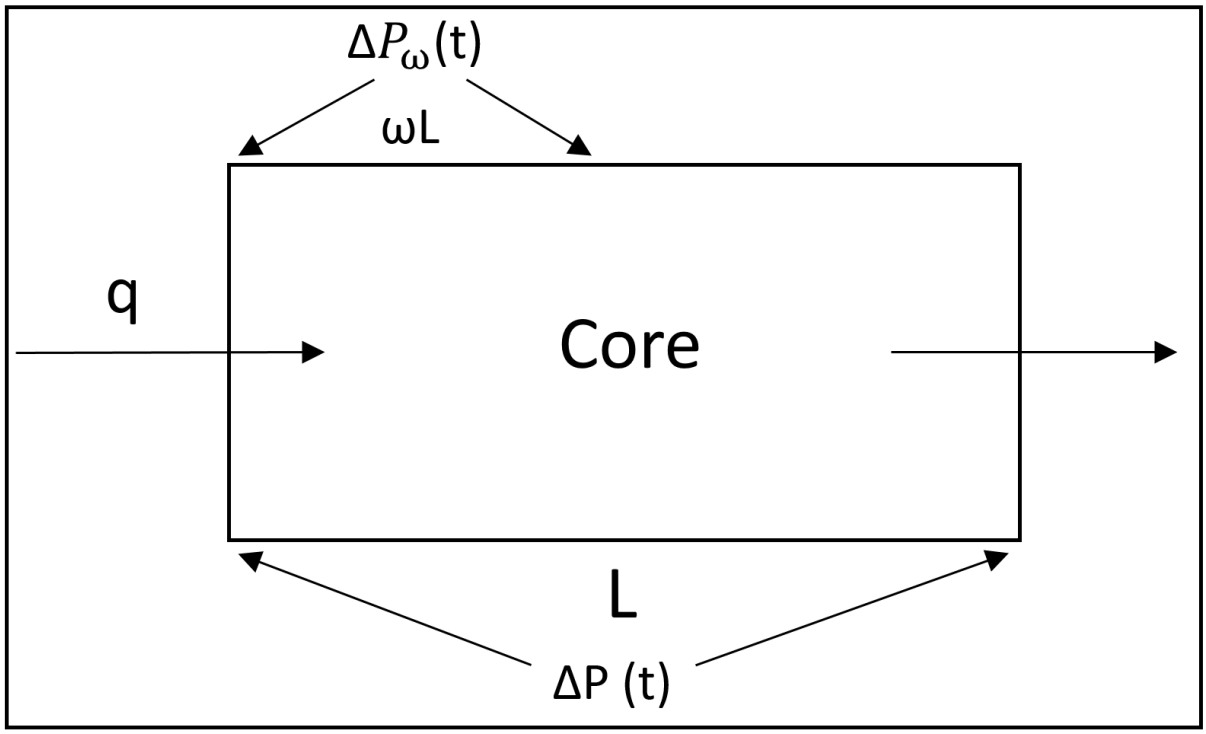

Figure 4.4 Illustration of how the three-point pressure method is performed

We can use this second slope, $m_{\omega,}$ to plot the formation damage coefficient as a function of filtration coefficient in the same graph as we did using the slope m. When we are plotting the relationship with $m_{\alpha,}$ the length of the core will now be shorter and L must now be expressed as ωL where ω is the position of the intermediate pressure point measurement.

$$m_\omega = \frac{II_0\beta\mu C_0(1 - e^{-\lambda\omega L})}{A^2 k_0} \quad \textit{Equation 4.17}$$

Values of m_ω and ω are not available for Grane well G-32, the values chosen to present the theory are approximate. Using these values in Equation 4.17 and plotting β as a function of λ in the same graph as we get this curve:

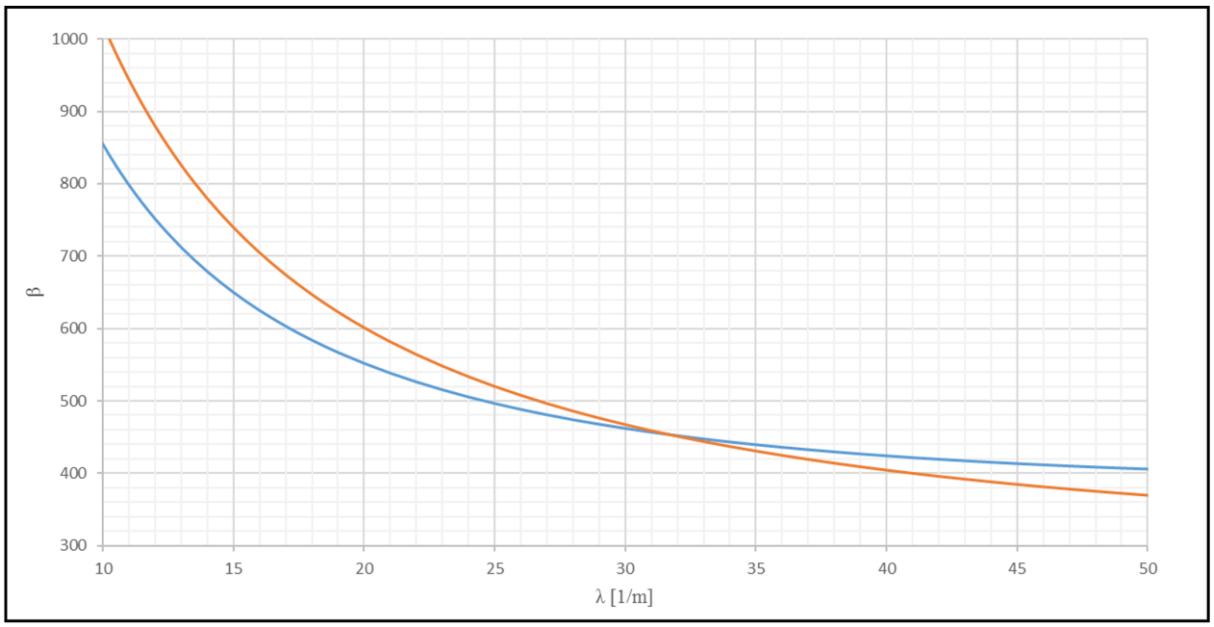

Figure 4.5 Formation damage coefficient as function of filtration coefficient using two different slopes in the same core

All the parameters are the same for both cores, and we get one value for each of the variables, and this is seen in the intersection between these two graphs.

The slopes are determined from the injectivity curve, which again are calculated from pressure drop measurement during laboratory test. A sensitivity analysis should be performed for the formation damage and filtration coefficient for small variations in the pressure data as the pressure measurements have limited accuracy. Experiments show that the small variations have little effect on β and λ and that the procedure is stable (Bedrikovetsky et al., 2002).

4.4.3 Changing filtration coefficient

The filtration coefficient changes with the amount of injected volume due to several effects. The deposited particles can act as collectors, and this increases the collection efficiency. The deposition of new particles will also reduce the porosity in that area and increase the velocity of the particles (more collisions between particles and grains gives higher collection efficiency) and change the flow field. Changes in the flow field results in previously deposited particles being picked up, and effectively decreasing the filtration coefficient. The filtration coefficient will be reduced if the surface forces are strongly repulsive, as this reduces the likelihood of particles attaching.

When particles continue to deposit inside the formation, bridging of pore throats will become a more and more important plugging mechanism until most of the pore throats are plugged.

After this the filter cake will start building up. Several investigations have been done to fit a function of the filtration coefficient to experimental data, and most of these functions are derived from a more general relation proposed by Ives (1969):

$$\frac{\lambda}{\lambda_0} = \left(1 + \frac{w_i \sigma}{\phi_0}\right)^{x_i} \left(1 + \frac{\sigma}{\phi_0}\right)^{y_i} \left(1 + \frac{\sigma}{\sigma_m}\right)^{z_i} \quad \text{Equation 4.18}$$

Where x_i, y_i, z_i and w_i are empirical variables, σ is the deposited particle concentration and σ_m is the maximum deposited particle concentration (Ison & Ives, 1969; Wennberg & Sharma, 1997).

4.5 External filtration

External filtration is when particles deposits on the inside of the borehole because particles are blocked from flowing into the formation. These deposited particles on the inside of the borehole make up the external filter cake. The injectivity will decrease with thicker filter cake. The important parameters of the filter cake are filter cake porosity and permeability. The lower these values are, the lower the injectivity will be.

Bechhold (1907) found that the amount of filtrate injected before a compact filter cake blocking the pores is created increased by having a parallel flow during the filtration process. Parallel flow corresponds to a crossflow scenario. A crossflow scenario is observed during PWRI in a hydraulically fractured reservoir. The flow of produced water will flow parallel to the fractures, and will therefore increase the volume of produced water that can be injected before a compact filter cake is made compared to perpendicular flow. Part of this reason is that crossflow gives rise to higher erosion, and gives particles higher chance to get transported into the formation (Bechhold, 1907; Farajzadeh, 2004).

Forces and mechanisms that determine internal and external filtration are mostly the same. Internal filtration does in a way create an internal filter cake inside the porous media in much the same way as a filter cake develops externally. Mechanism and forces behind governing external filtration will therefore not be further explained in this thesis.

4.6 Range for variation on injectivity damage parameters

The four injectivity damage parameters are the filtration coefficient (λ), formation damage coefficient (β), cake permeability (k_C) and cake porosity (ϕ_C). Bedrikovetsky (2005) found typical ranges of the different values based on different papers:

- λ – from 10 to 300 $\left(\frac{1}{m}\right)$
- β – from 50 to 1000
- k_c – from 0.03 md to 1 md

These values are found using core flood experiments, and these are presented in: (Al-Abduwani, de Zwart, Farajzadeh, van den Broek, & Currie, 2004; Bedrikovetsky et al., 2002; Da Silva et al., 2004; Herzig et al., 1970; Khatib, 1994; Pang & Sharma, 1997; Sharma, Pang, Wennberg, & Morgenthaler, 1997; Van den Broek, Bruin, Tran, Van der Zande, & Van der Meulen, 1999; Wennberg & Sharma, 1997).

The range listed above is the most normal range, and Bedrikovetsky (2007) did a core flood test with water containing small particles and got a λ equal to 1.9. The porosity of the filter cake is expected to be between 0.15 and 0.20 (Bedrikovetsky, Furtado, Siqueira, & de Souza, 2007; M.M. Sharma & Pang, 1997). Bedrikovetsky (2005) did get filter cake permeability equal to 10 mD during core flooding (Bedrikovetsky et al., 2005). β values up to 10^5 have also been recorded (Bedrikovetsky et al., 2002).

5 Pavel Bedrikovetsky's model for injectivity decline

Mathematical models for internal and external filtration have been developed by numerous authors like Sharma, Khatib and Wennberg. These models have been developed using core flood and field data. Bedrikovetsky adds the effect of external cake erosion, filling of the well by erosion products and initial increase of the injectivity index due to water displacing oil with higher viscosity. The model is implemented in the SPIN software (Simulates and Predicts the INjectivity) (Bedrikovetsky et al., 2007; Khatib, 1994; Pang & Sharma, 1997; Sharma et al., 1997).

The model for internal and external filtration is based on four parameters. The filtration- and formation damage coefficient, filter cake permeability and critical porosity fraction. The three constants that can be extracted from the well injectivity are the slope of the impedance curve during internal and external filtration and the transitional time. These three contestants are functions of the four parameters that the model uses.

This chapter is primarily based on SPE 100334 "A Comprehensive Model for Injectivity Decline Prediction During PWRI" (Bedrikovetsky et al., 2007).

5.1 Correlation between formation damage coefficient and critical porosity fraction

The formation damage coefficient is dependent on the pore space geometry inside the porous media, and not on the capturing mechanisms. The formation damage coefficient is primarily dependent on the ratio between the mean pore space and the particle size. The critical porosity fraction is also a function of the geometry inside the pore space and the particle diameter. One should therefore expect that the formation damage coefficient is dependent on the critical porosity fraction.

Da Silva et. al (2004) tried to find a correlation between the formation damage coefficient and the critical porosity using experimental data from core flood test done by Tran and Van den Broek (1998) and Van den Broek et. al. (1999). They obtained this correlation:

$$\beta = 95\alpha^{-0.41} \qquad \textit{Equation 5.1}$$

The correlation they observed had a high uncertainty with a R^2 value of 0.7032. This indicates that the correlation is more complex and dependent on other parameters, but can be used as an approximation (Bedrikovetsky et al., 2007; Da Silva et al., 2004; Tran & Van den Broek, 1998; Van den Broek et al., 1999).

5.2 Internal filtration

The model for internal filtration is derived using mass balance of suspended and deposited particles, particle capture kinetics and Darcy's law for permeability reduction due to retained particles:

$$\phi \frac{\partial C}{\partial t} + \frac{q}{2\pi r}\frac{\partial C}{\partial r} = -\frac{\partial \sigma}{\partial t} \qquad \textit{Equation 5.2}$$

$$\frac{\partial \sigma}{\partial t} = \lambda U C \qquad \textit{Equation 5.3}$$

$$U = -\frac{k_0 k_{rwor}}{\mu(1+\beta\sigma)}\frac{\partial P}{\partial r} \qquad \textit{Equation 5.4}$$

Where C is the particle concentration in produced water (vol/vol), t is the time (s), σ is the deposited particle concentration (vol/vol) and k_{rwor} is relative permeability for water at the presence of residual oil (m^2).

Dimensionless values are introduced for radius (r_D), time (t_D), concentration (C_D) and pressure (P_D):

$$r_D = \frac{r}{R_c} \qquad \textit{Equation 5.5}$$

$$t_D = \frac{1}{\phi \pi {R_c}^2}\int_0^t q(t)dt \qquad \textit{Equation 5.6}$$

$$C_D = \frac{C}{C_o} \qquad \textit{Equation 5.7}$$

$$P_D = \frac{2\pi k_0 k_{rwor} P}{\mu q} \qquad \textit{Equation 5.8}$$

Where R_C Is the half distance between injector and producer.

With the assumption that the filtration and formation damage coefficients are constant we get:

$$II = \frac{q(t)}{\Delta p(t)} \qquad \textit{Equation 5.9}$$

$$J(t_D) = \frac{II(0)}{II(t_D)} = \frac{\Delta P(t_D)}{\Delta P_0} \qquad \textit{Equation 5.10}$$

$$J(t_D) = 1 + mt_D \qquad \textit{Equation 5.11}$$

$$m = \frac{\beta\phi C_0(\lambda R_c)^2}{ln\left(\frac{R_c}{r_w}\right)}\left(\frac{1}{\lambda r_w} + e^{\lambda r_w}E(\lambda r_w)\right) \qquad \textit{Equation 5.12}$$

Where $E(\lambda r_w)$ is the error function. The detailed derivations are presented in (Bedrikovetsky et al., 2007)

Equation 5.12 is the one that is used in the SPIN model. A simplified version of Equation 5.12 is also available, and can be expressed as:

$$m = \beta\phi C_0(1 - e^{-\lambda}) \qquad \textit{Equation 5.13}$$

(Da Silva et al., 2004)

5.3 Transition time and external filtration

The particle deposition mechanics can be expressed by the suspended particle concentration in the injected fluid:

$$\sigma(r_w, t) = \frac{\lambda C_0 q}{2\pi r_w} t \qquad \textit{Equation 5.14}$$

The transition time (t_{tr}) is the time where plugging mechanism transition from internal filtration to external filtration. We say that the porosity has reached the critical porosity fraction (α) when the transition time is reached:

$$\alpha\phi = \frac{\lambda C_0 q}{2\pi r_w} t_{tr} \qquad \textit{Equation 5.15}$$

The transitional time can be calculated:

$$t_{tr} = \frac{2\alpha\phi\pi r_w}{\lambda C_0 q} \qquad \textit{Equation 5.16}$$

And the dimensionless transition time (t_{Dtr}) expressed in p.v.i. (pore volumes injected):

$$t_{Dtr} = \frac{2\alpha r_w}{\lambda {R_c}^2 C_0} \qquad \textit{Equation 5.17}$$

The pressure drop between the between the producer and injector at the transition time can be expressed as:

$$\Delta p(t_{Dtr}) = \frac{\mu q}{2\pi k_0 k_{rwor}} ln\left(\frac{R_c}{r_w}\right) J(t_{Dtr}) \qquad \textit{Equation 5.18}$$

The left side of the equation can be linearized with the assumption that the filter cake thickness is much smaller than the radius of the well ($h_c << r_w$), and obtain an equation for the filter cake thickness:

$$h_c(t) = \frac{C_0}{2\pi r_w(1-\phi_c)} \int_{t_{tr}}^{t} q(t)\, dt \qquad \textit{Equation 5.19}$$

$$h_c(t) = \frac{C_0 {R_c}^2 \phi (t_D - t_{Dtr})}{2 r_w (1-\phi_c)} \qquad \textit{Equation 5.20}$$

By using Darcy's law for flow through porous media we obtain an expression for the pressure drop across the filter cake, ΔP_c :

$$\Delta P_c = -\int_{r_{w-h_c}}^{r_w} \frac{\partial p}{\partial r} dr = \frac{q\mu_w}{2\pi k_c r_w} h_c \qquad \textit{Equation 5.21}$$

$$\Delta P_c = \frac{q\mu C_0 {R_c}^2 \phi (t_D - t_{Dtr})}{4\pi {r_w}^2 k_c (1-\phi_c)} \qquad \textit{Equation 5.22}$$

The dimensionless pressure drop across the filter cake can be obtained by using Equation 5.3 and Equation 5.22:

$$\Delta P_c = \frac{k_0 k_{rwor} C_0}{2 X_w k_c (1-\phi_c)} (t_D - t_{Dtr}) \qquad \textit{Equation 5.23}$$

Where X_w is the dimensionless well coordinate

The total pressure drop between the well and the reservoir is equal to the pressure drop in the porous media and the pressure drop through the filter cake. We then obtain an expression for the impedance for external filtration

$$J(t_D) = 1 + mt_{Dtr} + \frac{k_0 k_{rwor} C_0}{2X_w k_c (1-\phi_c)}(t_D - t_{Dtr}) \qquad \textit{Equation 5.24}$$

And the dimensionless slope during external filtration, m_c:

$$m_c = \frac{k_0 k_{rwor} C_0}{2X_w k_c (1-\phi_c)} \qquad \textit{Equation 5.25}$$

(Bedrikovetsky et al., 2007)

A simplified equation for the slope during external filtration:

$$m_c = \frac{k_0 C_0 \phi}{k_c (1-\phi_c)} \qquad \textit{Equation 5.26}$$

(Da Silva et al., 2004)

5.4 Injectivity increase during saltwater injection

A reservoir section saturated with oil will have lower mobility than water in the same reservoir due to the higher viscosity in oil than water. When saltwater is injected we will observe a injectivity increase due to the difference in viscosity. Using Buckley-Leverett for axi-symmetric flow an expression for the mobility ratio increase, M, can be found:

$$M = \frac{k_{rwor}\mu_o}{k_{rowi}\mu_w} > 1 \qquad \textit{Equation 5.27}$$

Where k_{rowi} is the relative permeability for oil at the presence of water. The detailed derivation can be seen in Bedrikovetsky et al. (2007).

The effect from different mobility in water and oil can be included in the model for predicting damage during internal and external filtration and we get a new expression for the impedance:

$$J(t_D) = \begin{cases} J_{BL}(t_D) + \dfrac{m}{M} t_D & t_D < t_{Dr} \\ J_{BL}(t_D) + \dfrac{m}{M} t_{Dtr} + \dfrac{m_c}{M}(t_D - t_{Dr}) & t_D > t_{Dr} \end{cases}$$

Where J_{BL} describes the impedance variation during particle free saltwater injection (Bedrikovetsky et al., 2007).

5.5 External filter cake erosion and filling due to erosion

Some wells do not follow the typical linear impedance curve model for external and internal filtration. After a high increase in the impedance during external filter cake formation the growth rate of the impedance slows down. This indicates that the filter cake starts to erode, and the linear impedance profile during external filtration is no longer valid. The filter cake starts to erode due to crossflow that gives the particle a drag force. Force balance must be done in order to obtain the equilibrium for filter cake thickness along the well. Lift, drag, diffusion and electrostatic forces will be considered. These forces are discussed further in chapter 3

Most particles will be transported into the rat hole when the filter cake thickness reaches equilibrium condition. The rat hole will eventually be filled, and the well itself will be gradually filled. The filling that occurs in the rat hole will have no effect on the injectivity and corresponds to a plateau impedance. The period of rat hole filling can be calculated using the volume of the rat hole, injection rate, amount of total suspended solids and the porosity of the deposit (Bedrikovetsky et al., 2007).

The injectivity index becomes more complicated to calculate when the rate hole is full and the well has started to fill up. The SPIN model uses a steady state model with crossflow into the reservoir and vertical flow in the well. The crossflow is based on Dupuit-Forchheimer equations with two different skin factors for internal and external filtration. The vertical flow that is observed in the upper section will follow Hagen–Poiseuille equations, while the lower part will follow Darcy's law (Bedrikovetsky et al., 2007; Wooding & Chapman, 1966).

6 Simple model for injectivity decline during produced water re-injection

This chapter present a simple model based on the work done by authors like Sharma, Khatib, Wennberg and Bedrikovetsky. The main difference between this model and previous models is that this model uses Cumulative Injected Volume (CIV (m^3)) instead of cumulative injected pore volumes (dimensionless). The effect of increasing the area the water is injected into is easier to observe with CIV. (Da Silva et al., 2004; Khatib, 1994; Pang & Sharma, 1997; Wennberg & Sharma, 1997).

6.1 Internal filtration.

From Sharma (1997) we have an equation for the concentration of particles dispersed in the fluid at a given depth x (m) inside the formation, C, under the assumption that the filtration coefficient is independent of the concentration of particles, and the filtration coefficient is constant:

$$C(x) = C_0 e^{-\lambda x} \qquad \textit{Equation 6.1}$$

Where C_0 is the injected solids consentration (vol/vol). From this we get a concentration profile of the particles:

$$\sigma(x,t) = \frac{q}{A} t C_0 \lambda e^{-\lambda x} \qquad \textit{Equation 6.2}$$

Where σ is the deposited particles concentration, q is the flowrate of water injected (m^3/s), A is area of the formation water is injected into (m^2) and t is the time variable. An expression can be made for the porosity change in the near wellbore region:

$$\phi(x,t) = \phi_0 - \sigma(x,t) \qquad \textit{Equation 6.3}$$

Where ϕ is the porosity of the formation and ϕ_0 is the initial porosity. Equation 6.3 describes how the porosity near wellbore changes as particles are injected into the formation. (Sharma et al., 1997)

An expression for the flow velocity, U, can be found with a modified version of Darcy's law that accounts for formation damage due to particle retention:

$$U = -\frac{k_0}{\mu(1+\beta\sigma(x,t))}\frac{dP}{dx} \quad \textit{Equation 6.4}$$

Where k_0 is the initial permeability (m^2), μ is the viscosity of the fluid (pas), β is the formation damage coefficient and p is pressure (bar) (Bedrikovetsky et al., 2002).

An expression for the pressure differential for internal filtration can be obtained by combining these equations:

$$V = qt \quad \textit{Equation 6.5}$$

Equation 6.2 + Equation 6.5:

$$\sigma(x,t) = \frac{V}{A}C_0\lambda e^{-\lambda x} \quad \textit{Equation 6.6}$$

Equation 6.4 + Equation 6.6:

$$U = -\frac{k_0}{\mu(1+\beta(\frac{V}{A}C_0\lambda e^{-\lambda x}))}\frac{dp}{dx} \quad \textit{Equation 6.7}$$

Equation 6.7 re-arranged:

$$\Delta P = \frac{U\mu}{k_0}\int_0^L dx + \frac{\beta U\mu V C_0\lambda}{Ak_0}\int_0^L e^{-\lambda x}dx \quad \textit{Equation 6.8}$$

$$U = \frac{q}{A} \quad \textit{Equation 6.9}$$

Equation 6.8 + Equation 6.9:

$$\Delta P = \frac{q\mu L}{Ak_0} + \frac{\beta q\mu V C_0(1-e^{-\lambda L})}{A^2k_0} \quad \textit{Equation 6.10}$$

Equation 6.10 is an expression of the pressure drop due to skin damage, and can be used to calculate the injectivity index (II) and the impedance (J):

$$II = \frac{\mathrm{q}}{\Delta P} \quad \textit{Equation 6.11}$$

$$\frac{1}{II} = \frac{\Delta P}{\mathrm{q}} \quad \textit{Equation 6.12}$$

$$J = \frac{II_0}{II} = \frac{II_0\Delta P}{\mathrm{q}} \quad \textit{Equation 6.13}$$

Equation 6.10 + Equation 6.12: $$\frac{1}{II} = \frac{\mu L}{Ak_0} + \frac{\beta \mu C_0 (1 - e^{-\lambda L})}{A^2 k_0} V$$ *Equation 6.14*

Equation 6.11 + Equation 6.12: $$J = \frac{II_0 \mu L}{Ak_0} + \frac{II_0 \beta \mu C_0 (1 - e^{-\lambda L})}{A^2 k_0} V$$ *Equation 6.15*

Where II_0 is the initial injectivity.

We can find an expression for II_0 by using Darcy's law, and insert it into Equation 6.15:

$$J = 1 + \frac{II_0 \beta \mu C_0 (1 - e^{-\lambda L})}{A^2 k_0} V$$ *Equation 6.16*

6.2 External filtration

We have Darcy's law for fluid passing through a filter cake under the assumption of linear flow:

$$\Delta P = \frac{\mu q_f h_c}{Ak_c}$$ *Equation 6.17*

Where q_f is the flowrate of the filtrate, h_c and k_c is the thickness and permeability of the filter cake respectively.

We also have that the amount of particles that is deposited must be equal to the amount of particles that are injected:

$$A_f h_c (1 - \phi_c) = C_0 \int q dt$$ *Equation 6.18*

The flowrate of the filtrate can be expressed by the flowrate and injected particle concentration:

$$q_f = q(1 - C_0)$$ *Equation 6.19*

The volume of the filter cake can be expressed by its area and height:

$$V = h_c * A$$ *Equation 6.20*

By combining the equations above we can get an expression for the impedance:

Equation 6.16 + Equation 6.17 + Equation 6.18:

$$\Delta P = \frac{\mu q h_c C_0 (1 - C_0)}{A k_c (1 - \phi_c)} \quad \textit{Equation 6.21}$$

Equation 6.21 + Equation 6.20:

$$\Delta P = \frac{\mu q (C_0 - {C_0}^2)}{A^2 k_c (1 - \phi_c)} V \quad \textit{Equation 6.22}$$

Equation 6.12 + Equation 6.22:

$$\frac{1}{II} = \frac{\mu (C_0 - {C_0}^2)}{A^2 k_c (1 - \phi_c)} V \quad \textit{Equation 6.23}$$

Equation 6.13 + Equation 6.22:

$$J = \frac{II_0 \mu (C_0 - {C_0}^2)}{A^2 k_c (1 - \phi_c)} V \quad \textit{Equation 6.24}$$

6.3 Concentration of solids

The concentration of solids (C_0) is a dimensionless variable usually given in ppm (10^{-6}). The amount of solids is however often given in Total Suspended Solids (TSS) given in mg/l. To calculate C_0 from TSS:

$$C_0 = \frac{TSS * 10^{-3}}{\rho_s} \quad \textit{Equation 6.25}$$

Where TSS are given in (mg/l), and ρ_s is the density of solids (kg/m^3).

6.4 Transitional volume

The theory of internal filtration is only valid to a certain point called the transitional volume, and from this point the theory of external filtration is valid. The transitional volume, V_{tr}, can be determined if you have the impedance graph, and V_{tr} will be the intersection between two linear lines.

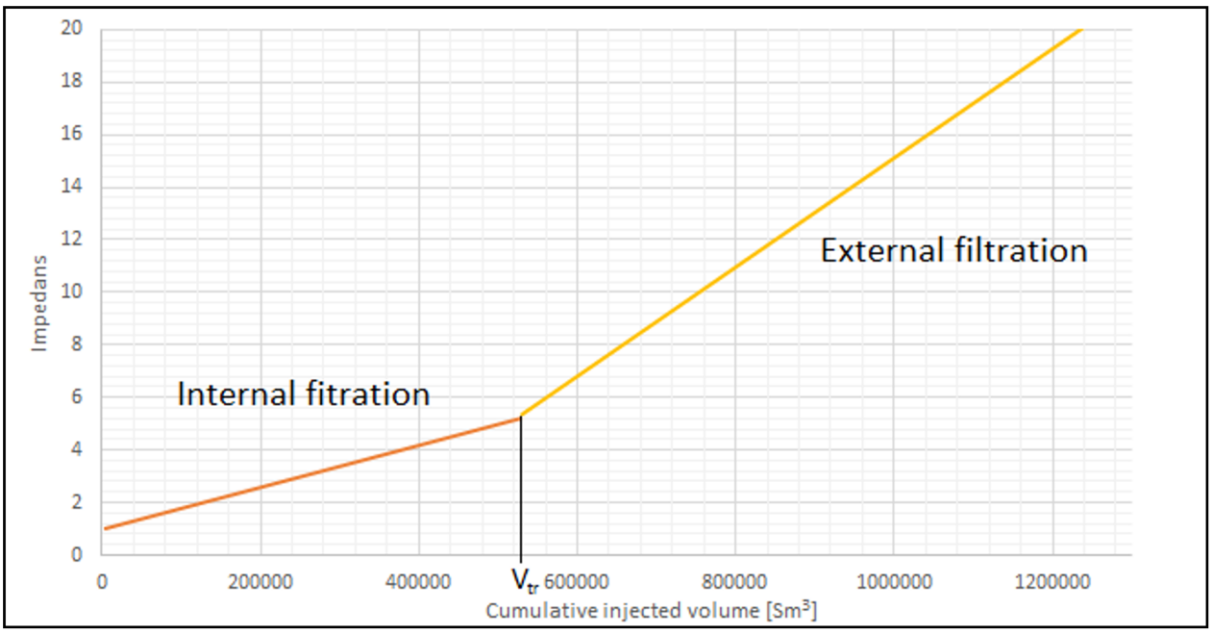

Figure 6.1 Transition volume between internal and external filtration during PWRI

Figure 6.1 Shows a typical impedance development curve, and this curve can be expressed by this formula:

$$J(V) = \begin{cases} 1 + mV & V < V_{tr} \\ 1 + mV_{tr} + m_c(V - V_{tr}) & V > V_{tr} \end{cases} \quad \textit{Equation 6.26}$$

Where m is the slope during internal filtration and m_c is the slope during external filtration:

$$m = \frac{II_0\beta\mu C_0(1 - e^{-\lambda L})}{A^2 k_0} \quad \textit{Equation 6.27}$$

$$m_c = \frac{II_0\mu(C_0 - {C_0}^2)}{A^2 k_c(1 - \phi_c)} \quad \textit{Equation 6.28}$$

We normally represent viscosity by cP, permeability by mD and Injectivity by m^3bar/day. A conversion factor can be applied to prevent unnecessary conversion to SI units. We get a conversion factor equal to:

$$\frac{1}{24 * 60 * 60 * 10^5 * 9{,}869233 * 10^{-13}} = 117.3$$

Using this conversion factor the slope of internal and external filtration can be expressed as:

$$m = \frac{117.3 * II_0\beta\mu C_0(1 - e^{-\lambda L})}{A^2 k_0} \quad \textit{Equation 6.29}$$

$$m_c = \frac{117.3 * II_0 \mu (C_0 - {C_0}^2)}{A^2 k_c (1 - \phi_c)}$$ *Equation 6.30*

6.5 The effect of fracturing

Fracturing of the reservoir is usually achieved in the early phase where only seawater is injected. Stresses will be induced due to the temperature difference between the cold seawater and the warm reservoir, resulting in a reduced pressure needed to fracture the reservoir. The injection often transitions gradually from seawater to produced water, as more and more water is produced from the reservoir. The temperature of the water will increase as more and more produced water is injected, and higher pressure is needed for fractures to propagate. The pressure needed to fracture the reservoir when injecting produced water is still lower than the original fracturing pressure as the produced water is colder than the formation.

Fracturing during injection is the most common injection method for produced water re-injection wells because a higher injectivity is achieved, compared to only using matrix injection.

The main reason that fracturing gives higher injectivity is the increased area that the produced water is injected into. This gives more area that needs to be plugged compared to only using matrix injection. When the injectivity decreases in a fractured well the pressure will start to build up and this gives new fractures that have not yet been plugged. The continuing of this effect means higher injection rates are possible in fractured reservoir over extended periods. Another effect that increases the injectivity is the crossflow that naturally occur in fractures. This crossflow erodes the filter cake along the fractures and gives a higher injectivity. This effect is described in section 4.5.

The new area that is in contact with the reservoir formation is needed to include the effect of fracturing along with the erosion due to crossflow. This area is not easy to find as the length, diameter and number of fractures is not known. These can be estimated with different fracturing models, but these models cannot predict theses values accurately. These models have problems predicting the orientation of the fractures (Detienne, Ochi, & Rivet, 2005; Perkins & Gonzalez, 1985)

6.6 Grane well G-32

Grane well G-32 was chosen to test the model discussed in the previous section, as this is one of the few datasets open to the public. A plot showing the injectivity ($q/\Delta P$) plotted against the cumulative injected volume is used as basis. Data points have been extracted using pen and ruler. This will result in some uncertainties, but a good approximation of the real data. The data is taken from OTC paper "Increasing Oil Recovery on the Grane Field with Challenging PWRI" (Tipura, Tjomsland, & Fagerbakke, 2013).

6.6.1 General information

Grane well G-32 was the first Produced water re-injector well in the Heimdal formation on the Grane field. It was indicated that this well would improve the oil recovery for the nearby oil producers by lifting the Oil Water Contact (OWC) and Gas Oil Contact (GOC). The data used in this thesis is taken from (Tipura et al., 2013).

The sand in the Heimdal formation is generally interpreted as a high density turbidite sandstone with grains that are fine to medium, and moderate to well sorted. Other important parameters are listed in the table below:

Parameter	Value	Unit
Initial permeability	5-10	Darcy
Initial porosity	0.33	
Temperature	80	^{o}C
Initial BHP	176	Bar
Depleted BHP	140	Bar
Density of oil	984	Kg/m^3
Viscosity of Oil	10-12	cP
Injection interval	151.75	m
Wellbore diameter	8.5	Inches

Table 6.1 Important parameters for Grane well G-32

The purpose of the injector is not only to remove the produced water, but also to increase oil production. With fracture injection you do not have full control were you inject water, and you could end up injecting water into the oil zone, unflooded reservoirs or you could end up fracturing the cap rock and injecting water above the reservoir section. Matrix injection is a

better alternative to increase sweep efficiency, especially as Grane have one of the heaviest oils in the Norwegian Sea. Matrix injection means injecting at a pressure below the fracturing pressure and water is injected into the reservoir formation adjacent to the borehole.

Matrix injection is very hard to achieve, as plugging will reduce the injectivity and pressure must be increased to inject the same amount of water, which could result in the well fracturing. This makes Grane well G-32 one of the few wells that are chosen not to be fractured. To be able to have matrix injection over a longer period the amount of TSS and OIW should be as low as possible to increase the injectivity. This means increasing the cost for separators offshore.

Different injections rate of produced water is simulated to find the optimum injection rate to improve the production from nearby production wells. The optimum in this case is found to be an alternating injection rate between 2500Sm^3/day and 3000 Sm^3/day. The total injected amount of water planned to be injected is estimated to be 2.3 million Sm^3.

The quality of the produced water was not continuously monitored, but was sampled at two different occasions. The first was just after observing some instabilities in the separation process in January 2010 and the other was during stable process conditions in march 2010.

Month	OIW (mg/l)	TSS (mg/l)	Average particle diameter (by volume)
January	53-65	4-9	5 µm
March	18-22	2-9	3 µm

Table 6.2 Oil in water, total suspended solids and average particle diameter on Grane well G-32

The high measurement of OIW is not representative of the average OIW during injection as this was right after some instabilities, and the measurement of the OIW that was taken in march is more representative (Tipura et al., 2013).

6.6.2 Impedance for Grane well G-32

Data extracted from the graph showing injectivity decline in OTC paper "Increasing Oil Recovery on the Grane Field with Challenging PWRI" (Tipura et al., 2013):

Injectivity ($(Sm^3/day)/bar$)	Cumulative injected volume (Sm^3)
850	850000
725	725000
500	500000
400	400000
300	300000
200	200000
150	150000
100	100000
45	45000
30	30000

Table 6.3 Injectivity development on Grane well G-32

By plotting the data in the table above we get:

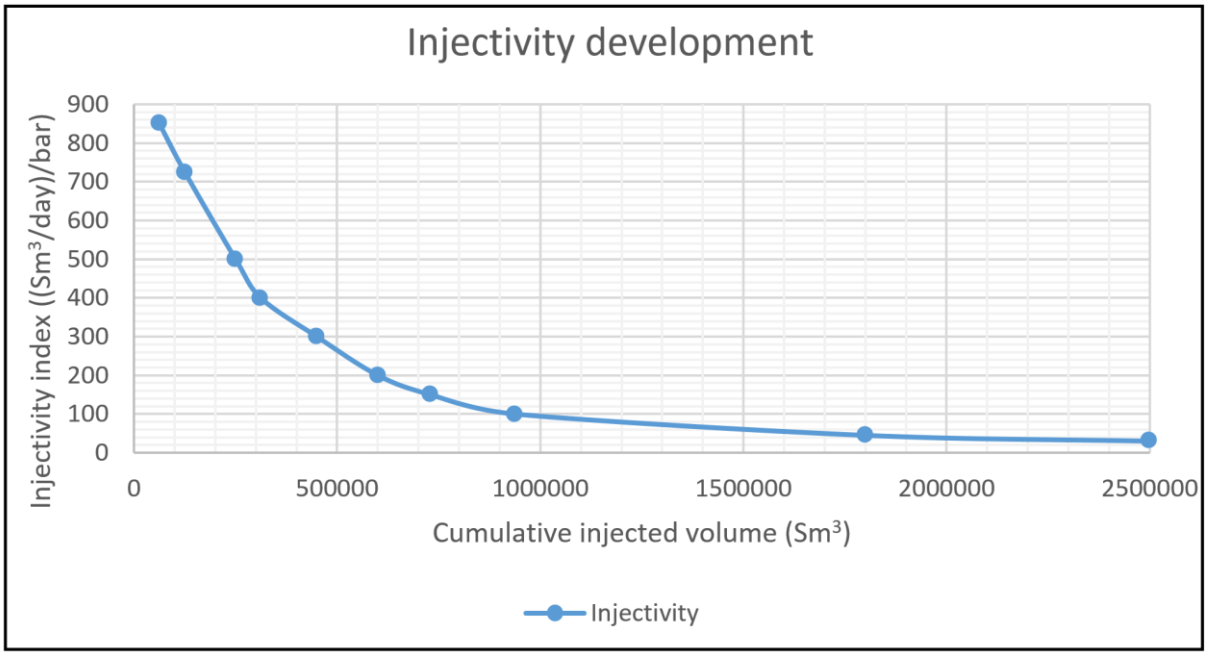

Figure 6.2 Injectivity development on Grane well G-32

In the original figure there are some data points that does not follow the overall trend, and these are not considered.

According to theory the inverse of the injectivity should give a linear trend (Bedrikovetsky et al., 2002). We should be able to see a transition between internal and external filtration if this is the plugging model representable for Grane well G-32. We use the method of least square fit, described in appendix A, to get a straight line that fit the data points best. The inverse of the injectivity index is plotted against the cumulative injected volume:

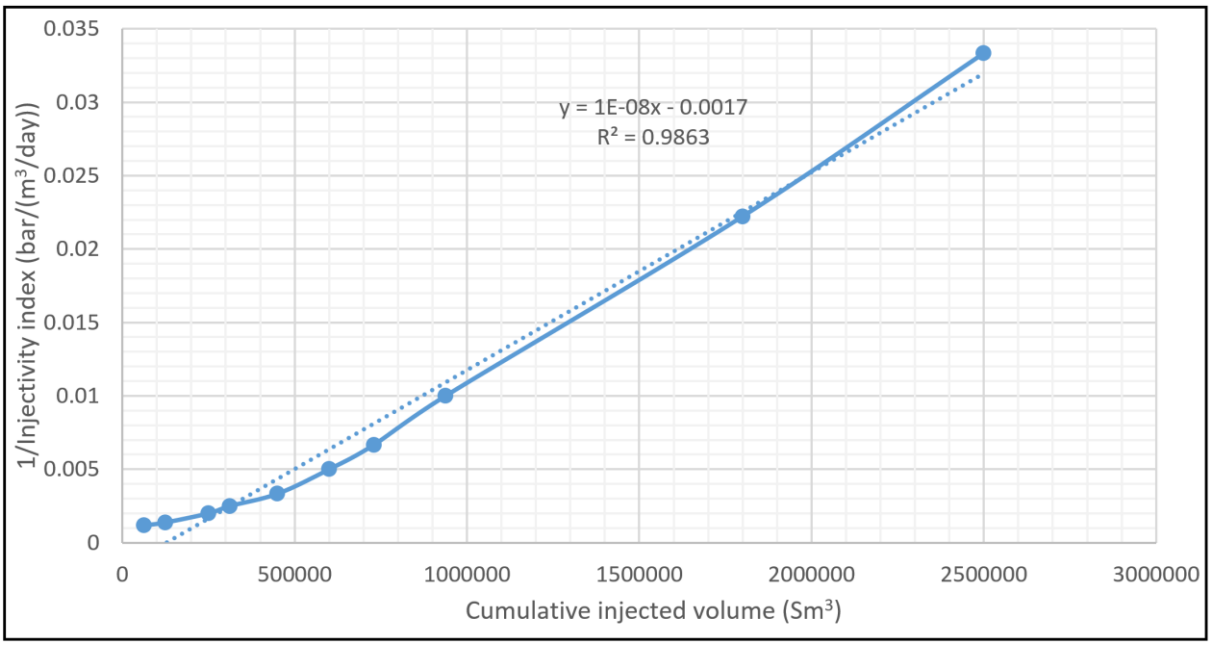

Figure 6.3 Development of the inverse of injectivity on Grane well G-32

We observe that the graph gives a linear trend with an R^2 value of 0.9863 using the method of least square fit. But we see that the first points have a bad correlation. This could be the case if there is a transition between internal and external filtration. To see if two independent curves give a better correlation the datasets is divided into two parts. The first five points and the rest:

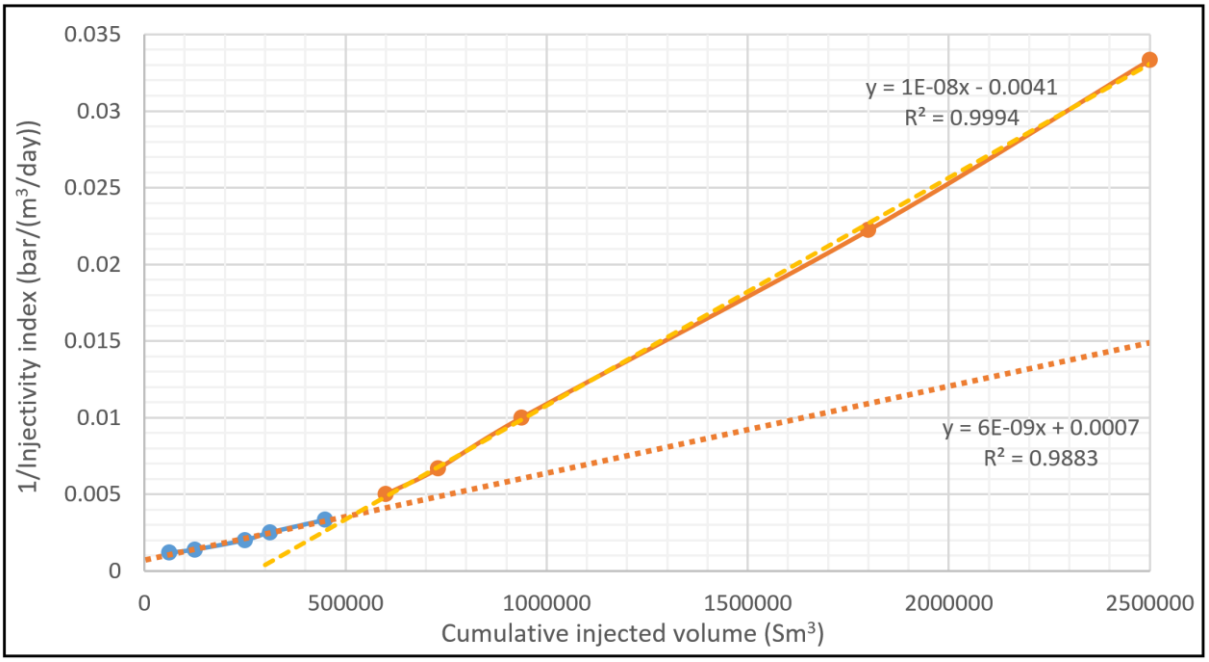

Figure 6.4 Inverse of injectivity index with internal and external filtration development on Grane well G-32

From this curve we see trends expected from internal filtration and external filtration. The simple model derived in chapter 6 is then assumed applicable for this dataset. For internal filtration we have this equation shown in section 6.1

$$J = 1 + \frac{II_0 \beta \mu C_0 (1 - e^{-\lambda L})}{A^2 k_0} V \qquad \textit{Equation 6.16}$$

If we divide the injectivity index with the initial injectivity index, we should get an intersection in the coordinates (1.0). We can use this information to back calculate the initial injectivity index not given in the paper. The current intersection in Figure 6.4 is at $7.177*10^4$ bar/(m^3/day). This gives that:

$$II_0 = \frac{1}{7.177 * 10^4} = 1393.4 \frac{bar}{\frac{m^3}{day}} \approx 1400 \frac{bar}{\frac{m^3}{day}}$$

Using this information, we can get a curve for the impedance:

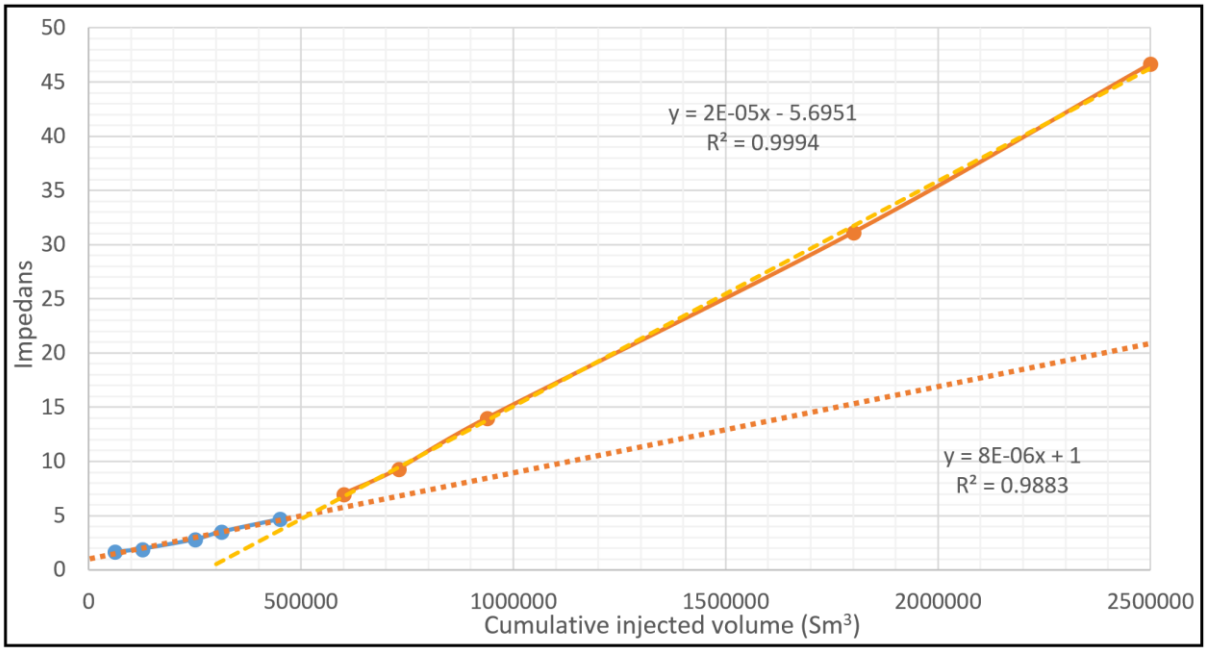

Figure 6.5 Impedance plotted against CIV on Grane well G-32

6.6.3 Total collection efficiency for Grane well G-32

Several parameters are necessary to calculate the total collection efficiency from Equation 4.14. These values will be discussed here. The velocity of the produced water containing particles can be calculated by using the length of the reservoir interval, porosity, diameter of hole and the injection rate. The velocity of produced water and particles are here assumed to be equal.

It was given that the Grane well G-32 could have an initial injection rate of 4000m^3/day. Using the data provided in Table 6.1 we get a fluid velocity of 0.0015 m/s when entering the formation. This is under the assumption that we have the same velocity over the entire reservoir interval. This will be entirely correct as the pressure differential will be higher at the heel of the reservoir section and lower at the toe.

The density of the particle is assumed to be 2650kg/m^3, and is the same as SiO_2 (normal sand). The average grain diameter of the reservoir formation is assumed to be 1000µm. The density and viscosity of fluid is assumed equal to that of seawater.

The collection efficiency describes the probability of particle deposition. More information about the collection efficiency is in section 4.3 and 4.4. Table with values used to calculate the collection efficiency:

D_g	Diameter grain	1000	μm
ρ_p	Density of particles	2650	kg/m^3
p_f	Density of fluid	1003	kg/m^3
μ	Viscosity of fluid	0.001	Pas
U	Velocity of fluid and particle	0.0015	m/s
φ	Porosity	0.33	
T	Temperature	80	^oC
		353.15	K

Table 6.4 Parameters used to calculate the collection efficiency

We can calculate the collection efficiencies as a function of the particle diameter using equations provided in section 4.3. We consider Interception, Impaction, Sedimentation, Diffusion and Electrostatic forces as different mechanisms leading to particle deposition. By using the equation provided for each of these mechanism as well as the total collection efficiency we get:

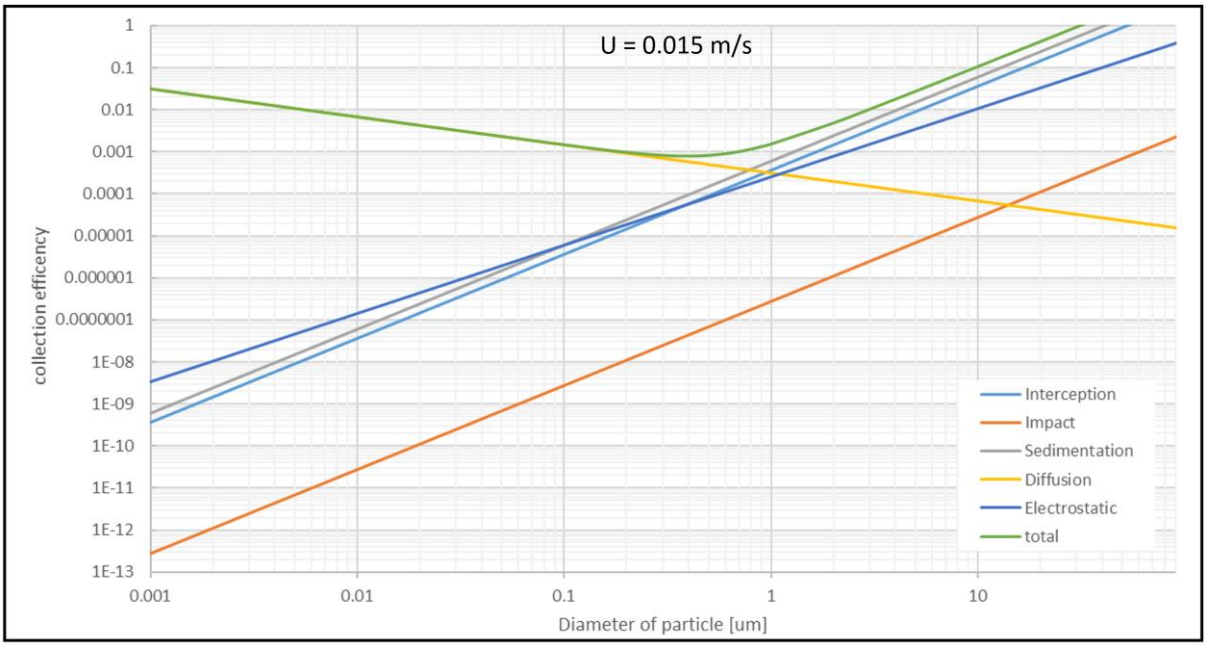

Figure 6.6 Collection efficiency at different grain diameters for Grane well G-32

We can see from *Figure 6.6* that diffusion is the dominating capture mechanism for particles up to a diameter of 0.8 µm and sedimentation for higher diameters due to the low velocity. The effect of interception, impact and electrostatic can be neglected in this case. Particles that are bigger than 23 µm will in this case have a 100% chance to settle out of the flow, and should therefore be avoided. If the velocity was increased to 0.05 m/s we would have this curve instead:

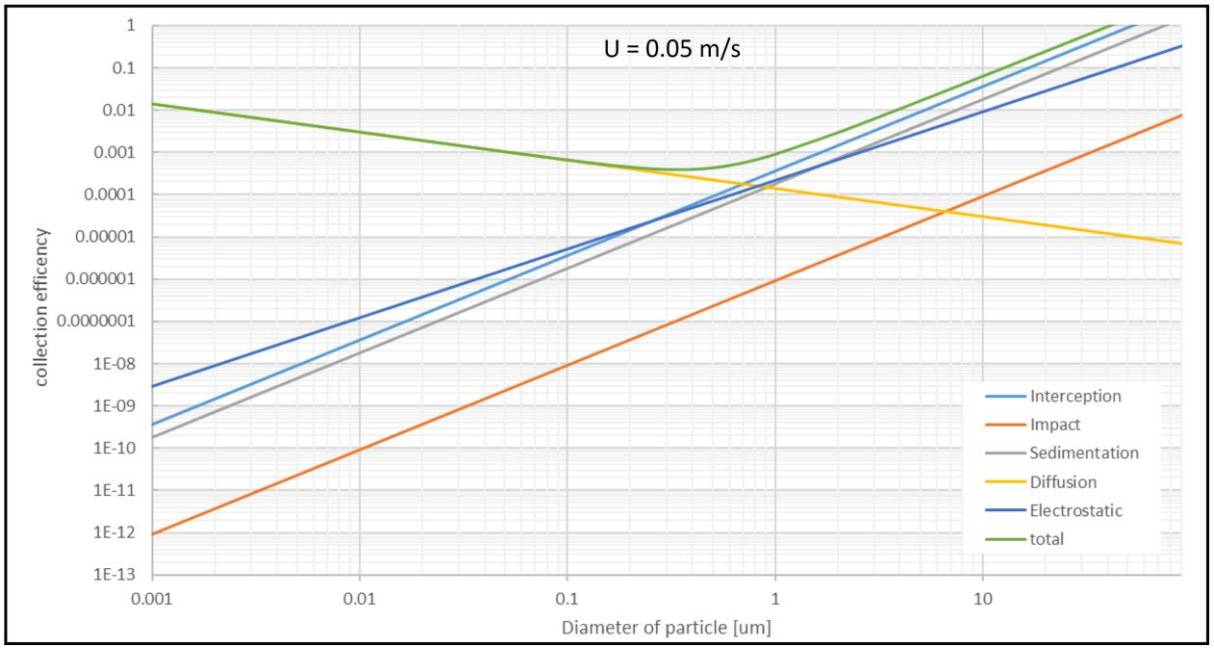

Figure 6.7 Collection efficiency for Grane well G-32 using a velocity of 0.05 m/s

We can observe a lower overall collection efficiency with a flow velocity of 0.05 m/s. The dominating force in this case is interception for particles bigger than 0.7 microns. Increasing the flow velocity could be achieved by increasing the injection rate of produced water.

A velocity of 0.05 m/s may not be optimal even if the collection efficiency is lowest at a velocity around 0.05 m/s, this only takes into consideration collection efficiency for each grain at initial conditions. As more and more particles are injected, bridging is more important, and higher velocity gives higher chance of bridging to occur. The most critical effect of increasing the injection rate is the pressure increase this results in. Higher pressure could cause fracturing, and should be avoided as this results in lower sweep efficiency.

The average particle diameter measured by volume is 5 microns in the test from January and 3 microns in the test taken in March. An average between these months have been chosen, even if the values in January were taken right after an inconsistency were observed in the separator.

This inconsistency mainly had an effect on the OIW. With a particle diameter of 4 microns we get than the total collection efficiency is equal to 0.00224.

Several of the formulas that is used to calculate the total collection efficiency is not linear with respect to particle diameter on a non-logarithmic scale as seen below:

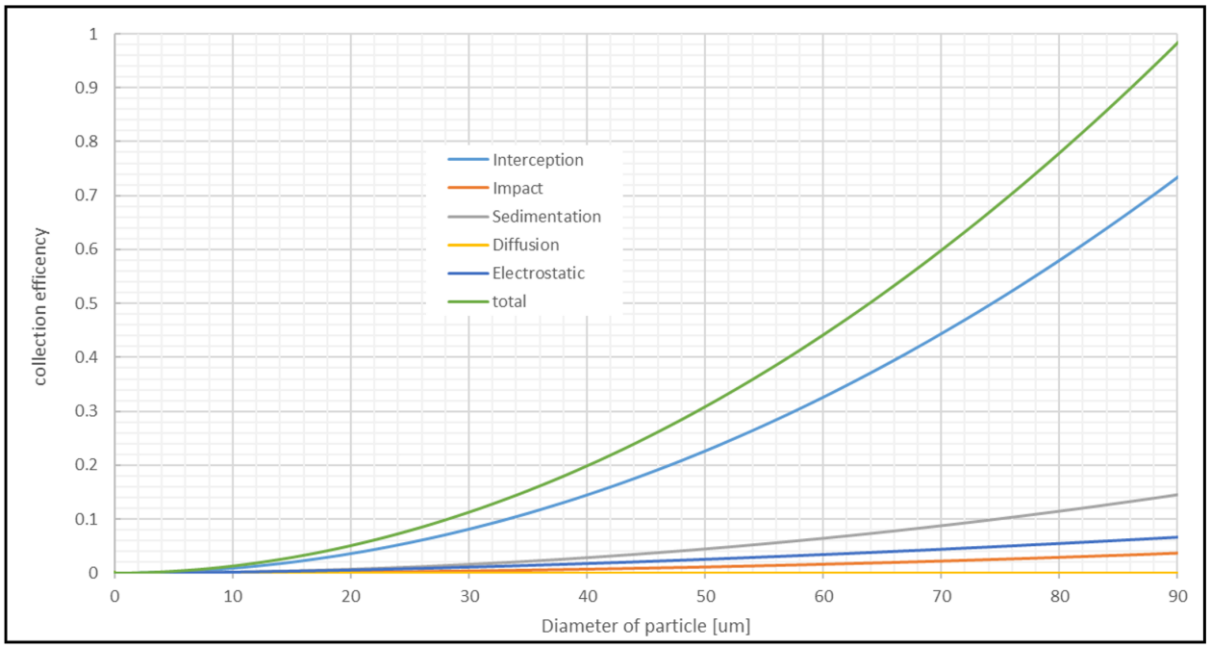

Figure 6.8 Collection efficiency on a non-logarithmic scale for Grane well G-32

To calculate more accurately the total collection efficiency, the total particle distribution should be used.

We do not have the total particle distribution, but it is given that the sample taken in January were 50% of the particles less than 5 microns and 75% less than 10 microns. While in March 50% of the particles less were than 3 microns and 80-90% less 10 microns. Combining these two measurements we get that 50% of the particles were less than 4 microns and 80% less than 10 microns.

Particles can from this be divided into three groups: less than 4 microns, between 4 and 10 microns and larger than 10 microns. The average values of these groups are assumed, and the collection efficiency corresponding to the diameter is calculated:

Average particle diameter size (μm)	Probability	Collection efficiency
3	0.50	0.0013
8	0.30	0.0085
12	0.20	0.0188

Table 6.5 probability and collection efficiency to different particle diameters

The average diameter sizes given in Table 6.5 are a high estimation as the higher values have higher impact on the total collection efficiency.

Using the three different collection efficiency and probability we get a total collection efficiency of:

$$\eta = 0.5 * \ 0.0013 + 0.3 * \ 0.0085 + 0.2 * 0.0188 = 0.0070$$

6.6.4 Filtration coefficient for Grane well G-32

Using a total collection efficiency of 0.0070 in Equation 4.15 we get the initial filtration coefficient equal to:

$$\lambda_0 = \frac{3\eta(1-\phi)^{\frac{1}{3}}}{2d_g} = \frac{3 * 0.0070(1-0.33)^{\frac{1}{3}}}{2 * 1000 * 10^{-6}} = 9.19\ m^{-1}$$

We are missing some important information to see if the simple model described in chapter 6 is representative for Grane well G-32. This is the formation damage coefficient, filter cake permeability and filter cake porosity, which all should be determined from laboratory experiments. The length L is in case of laboratory experiments the length of the core that were used to measure λ and β, and is in our case the length from the borehole and into the reservoir where plugging that affects the injectivity occur. This is usually a very low value, and is assumed to be 6 cm in our case.

6.6.5 Concentration of solids on Grane well G-32

This section will calculate C_0 form TSS. From Table 6.1 we have:

Month	TSS (mg/l)
January	4-9
March	2-9

Table 6.6 TSS on Grane G-32

TSS will be considered for both months and an average between them gives a TSS of 6 mg/l. From section 6.3 we have that:

$$C_0 = \frac{TSS * 10^{-3}}{\rho_s} \qquad \textit{Equation 6.25}$$

Using these values for TSS, a density of solids of 2650kg/m^3 we get that C_0 will be between 7.5*10^{-7} and 3.4*10^{-6} with an average value of 2.2*10^{-6}.

6.6.6 Formation damage coefficient, filter cake- porosity and permeability

β and $k_c(1-\phi_c)$ will be back calculated using the slope during internal and external filtration and then see if these values are realistic. By rearranging Equation 6.29 and Equation 6.30 we get:

$$\beta = \frac{mA^2 k_0}{117.3 * II_0 \mu C_0 (1 - e^{-\lambda L})} \qquad \textit{Equation 6.31}$$

$$k_c(1-\phi_c) = \frac{117.3 * \mu(C_0 - {C_0}^2) II_0}{m_c A^2} \qquad \textit{Equation 6.32}$$

The values used in Equation 6.31 and Equation 6.32 can be seen in the table below:

Parameter	Value	Unit
k_0	7.5	Darcy
m	$7.95*10^{-6}$	
A	102.9	m^2
μ	1.002	cP
II_0	1400	$(bar*day)/m^3$
C_0	$2.2*10^{-6}$	
L	0.06	m
m_c	$2.08*10^{-5}$	

Table 6.7 Values used to calculate β and $k_c(1-\phi_c)$

The initial permeability is an average value from Table 6.1, the slope from internal and external filtration is extracted from

Figure 6.5 and the area is calculated using the length of injection interval and borehole diameter from Table 6.1.

Inserting values for Grane well G-32:

$$\beta = \frac{7.95 * 10^{-6} * 102.9^2 * 7500}{117.3 * 1400 * 1.002 * 2.2 * 10^{-6}(1 - e^{-9.19*0.06})} = 4002$$

$$k_c(1 - \phi_c) = \frac{117.3 * 1.002(2.2 * 10^{-6} - (2.2 * 10^{-6})^2)1400}{2.08 * 10^{-5} * 102.9^2} = 1.69\ mD$$

6.7 Varying the injection interval

By assuming all other parameters except the slope during internal and external filtration stay constant we can calculate the injectivity development if we double the injection interval. The area will then be doubled to 205.8. We have from section 6.4:

$$J(V) = \begin{cases} 1 + mV & V < V_{tr} \\ 1 + mV_{tr} + m_c(V - V_{tr}) & V > V_{tr} \end{cases} \quad \textit{Equation 6.26}$$

Where m is the slope during internal filtration and m_c is the slope during external filtration and inserting values:

$$m = \frac{117.3 * II_0 \beta \mu C_0 (1 - e^{-\lambda L})}{A^2 k_0} = 1.99 * 10^{-6} \quad \textit{Equation 6.29}$$

$$m_c = \frac{117.3 * II_0 \mu (C_0 - {C_0}^2)}{A^2 k_c (1 - \phi_c)} = 5.20 * 10^{-6} \quad \textit{Equation 6.30}$$

We observe that the slopes in this case is exactly four time lower than the original slope, this can also be seen from equations above without inserting values as the area is squared. We can from this conclude that increasing the area produced water is injected into is an efficient way of reducing the injectivity significantly, and by this prolonging the life of an injection well.

6.8 Effect of fracturing

Fracturing was to be avoided during produced water re-injection into Grane well G-32, but it was stated in the report that some fracturing may have happened. If this was the case, we would expect to see a deviation from the linear trend in the impedance when the fracturing occurred. This was not observed, and indicates that the fracture did not occur or was too small to be have any visible effect on the impedance. It is possible that the fracturing did occur but the pressure was later reduced until the fracture closed again, and the fracturing corresponds to some of the values of the injectivity curve.

7 Discussion and conclusion

Discussion and conclusion regarding the simple model presented in chapter 6 and the method of determining the filtration coefficient in chapter 4 will be presented in this chapter. Recommendations for further work within PWRI are presented at the end of this chapter.

7.1 Discussion

The model derived in chapter 6 will be discussed in this section, divided into the part containing the internal filtration and the part containing external filtration.

7.1.1 Internal filtration

The filtration (λ) and formation damage coefficient (β) are needed for predicting injectivity damage using the model described in the previous chapter. λ is usually measured using the three-point pressure method, and not by Equation 4.15 presented in 4.4.1. There are more assumptions behind Equation 4.15 than the three-point pressure method. β is not available for Grane well G-32, and is back calculated. This value should be reasonable if the model is applicable.

We observed a filtration coefficient of 9.19, while the normal range described by Bedrikovetsky (2005) was between 10-300. However, Bedrikovetsky (2005) also found a filtration coefficient of 1.9 during core flooding (Bedrikovetsky et al., 2005). This indicates that the filtration coefficient is lower than expected, but still reasonable. A possible reason for the low filtration coefficient is the relatively low average diameter of solids injected. Fitzpatrick and Spielman (1973) found that increasing the diameter of injected solids increases the filtration coefficient. The Heimdal formation on Grane has a reservoir with high porosity this indicates a low filtration coefficient. Fitzpatrick and Spielman (1973) did experiments with two samples with a porosity of 0.38 and 0.41. They found that a porosity increase of 0.03 corresponded to a 30% decrease in λ (Fitzpatrick & Spielman, 1973).

The formation damage coefficient is back calculated to be 4002. The typical range for β is between 50 and 1000 (Bedrikovetsky et al., 2005). We observe we are not inside the expected range. Values of β up to 10^5 have been reported (Bedrikovetsky et al., 2002), and we cannot exclude that this β real. This β was back calculated using the filtration coefficient, and the reason we get a high β can be due to a too low estimate of λ, as β is a function of λ shown in Figure 4.3 when back calculating.

Assumed variables include the grain diameter, length of formation damage and density of particles. These values give an uncertainty of the result. Grain diameter will affect the filtration coefficient through the collection efficiency. Length of formation damage and density of particles will affect the back calculated formation damage coefficient.

Assumptions made in the derivations of the equations give uncertainties in the model. The assumption that λ is constant and equal to the initial filtration coefficient is questionable, as straining is not included. The Happel's cell model described in section 4.4.1 for calculating λ uses simplified pore space geometry, and this affects the validity of λ. The effect due to mobility difference between oil and water described in section 5.4 is not included in this model and can give a small error. The filtration should be measured using the three-point pressure method and compared to the calculated coefficients to evaluate the validity of the calculated λ.

7.1.2 External filtration

The porosity and permeability of the filter cake is needed for predicting injectivity decline with external filtration. These two values are not available for Grane well G-32, and are back calculated using the model presented in chapter 6.

When we back calculate we get $k_c(1-\phi_c) = 1.69\ mD$. We would expect the porosity to be in the range between 0.15 and 0.2, and that the permeability is expected to be between 0.03-0.1 mD (Bedrikovetsky et al., 2005). We get that $k_c(1-\phi_c)$ should be between 0.024 and 0.08 mD. We see that we are a factor of 70 higher than the highest estimate. We observe that the high value must be in the permeability, as this must be higher than 1.69 mD ($k_c = 1.69\ mD$ if $\phi_c = 0$). High values are not unheard of, and Bedrikovetsky (2005) measures a filter cake permeability of 10mD (Bedrikovetsky et al., 2005). This high value corresponds to $k_c(1-\phi_c)$ between 9 and 8.5. A $k_c(1-\phi_c)$ value of 1.69 mD does seem possible.

We observe a high cake permeability. If this is realistic or not could be determined using experiments to decide the cake porosity and permeability. A high value of the slope during external filtration (m_c) is usually observed. m_c on Grane well G-32 is lower than we would expect for similar plots in the literature (Bedrikovetsky et al., 2007). This low m_c value can be the reason we get a higher filter cake permeability.

7.2 Conclusion

The filtration coefficient (λ) was calculated as described in section 4.4.1. λ gave a lower value than expected, but this can be due to small particle diameter. This gives an indication that this method of determining λ can be a reasonable approximation when lacking core flood data, but is uncertain as a "true" λ is not available

The model presented in chapter 6 uses cumulative injected volume as the variable instead of pore volumes injected as presented in most models. This gives the possibility to estimate the injectivity change for different completion lengths. The model was tested on data taken from Grane well G-32. The formation damage coefficient (β), filter cake porosity (ϕ_c) and permeability (k_c) was back calculated to test the validity. β was higher than expected, but cannot be excluded due to higher values mentioned in literature. k_c gave a higher value than expected, but within reason. We can from this conclude the simple model to be realistic, but needs more data to say for sure.

7.3 Recommendations for further work

The model derived in chapter 6 was only tested for the data available for Grane well G-32 due to the lack of other datasets. There was no information about laboratory experiments to determine the porosity and permeability of the reservoir, the formation damage and filtration coefficient. Laboratory experiment using the three-point pressure method to determine the formation damage and filtration coefficient in sandstone similar to the reservoir rock could be done to test the model further. Experiments to determine the porosity and permeability of the filter cake based on the information given about the produced water should also be considered. Writing a thesis for a company where more data is available will give more opportunities for further analysis.

The effect of oil on injectivity decline could be investigated by varying the amount of oil injected during these experiments. The results from these experiments could give a direct correlation that can be used to model injectivity decline more correctly.

Polymers are more and more commonly injected into the formation for enhanced oil recovery during seawater injection or produced water re-injection. These polymers can be back produced into the produced water. The effect these chemical have on the injectivity are not fully understood, and laboratory experiments can be done in order to get better understanding how these chemicals affect the injectivity.

The injection tubing releases rust particles that decrease the injectivity. Experiments can be done in order to determine the amount and size distribution of these rust particles that are released per unit length of different casing types. Laboratory experiments can then determine the effect these rust particles have on the injectivity.

8 References

Al-Abduwani, F. A., de Zwart, B.-R., Farajzadeh, R., van den Broek, W., & Currie, P. K. (2004). *Utilising static filtration experiments to test existing filtration theories for conformance.* Paper presented at the 2nd Produced water workshop. Aberdeen, UK, 21st–22nd April.

Barkman, J. H., & Davidson, D. H. (1972). Measuring water quality and predicting well impairment. *Journal of Petroleum Technology, 24*(07), 865-873.

Batchelor, G. (1976). Brownian diffusion of particles with hydrodynamic interaction. *Journal of Fluid Mechanics, 74*(01), 1-29.

Bechhold, H. (1907). Kolloidstudien mit der Filtrationsmethode. *Zeitschrift für Elektrochemie und angewandte physikalische Chemie, 13*(32), 527-533.

Bedrikovetsky, P., Fonseca, D., Da Silva, M., Siqueira, A., de Souza, A., & Alves, C. (2005). *Well-History-Based Prediction of Injectivity Decline in Offshore Waterfloods.* Paper presented at the SPE Latin American and Caribbean Petroleum Engineering Conference.

Bedrikovetsky, P., Tran, P., Van den Broek, W., Marchesin, D., Rezende, E., Siqueira, A., . . . Shecaira, F. (2002). *Damage characterization of deep bed filtration from pressure measurements.* Paper presented at the International Symposium and Exhibition on Formation Damage Control.

Bedrikovetsky, P., Vaz, A., Furtado, C., & Serra de Souza, A. (2011). Formation-damage evaluation from nonlinear skin growth during coreflooding. *SPE Reservoir Evaluation & Engineering, 14*(02), 193-203.

Bedrikovetsky, P. G., Furtado, C. J. A., Siqueira, A., & de Souza, A. L. S. (2007). *A comprehensive model for injectivity decline prediction during PWRI.* Paper presented at the European Formation Damage Conference.

Belfort, G., Davis, R. H., & Zydney, A. L. (1994). The behavior of suspensions and macromolecular solutions in crossflow microfiltration. *Journal of Membrane Science, 96*(1-2), 1-58.

Bellarby, J. (2009). *Well completion design* (Vol. 56): Elsevier.

Collins, A. (1975). *Geochemistry of oilfield waters* (Vol. 1): Elsevier.

Da Silva, M., Bedrikovetsky, P., Van den Broek, W., Siqueira, A., & Serra, A. (2004). *A new method for injectivity impairment characterization from well and coreflood data.* Paper presented at the SPE Annual Technical Conference and Exhibition.

Detienne, J., Ochi, J., & Rivet, P. (2005). *A simulator for produced water re-injection in thermally fractured wells.* Paper presented at the SPE European Formation Damage Conference.

Faksness, L.-G., Grini, P. G., & Daling, P. S. (2004). Partitioning of semi-soluble organic compounds between the water phase and oil droplets in produced water. *Marine pollution bulletin, 48*(7), 731-742.

Farajzadeh, R. (2004). Produced Water Re-Injection (PWRI), an Experimental Investigation into Internal Filtration and External Cake Build-up. *Faculty of Civil Engineering and Geosciences*.

Fitzpatrick, J. A., & Spielman, L. A. (1973). Filtration of aqueous latex suspensions through beds of glass spheres. *Journal of colloid and interface science, 43*(2), 350-369.

Fox, R. W., & McDonald, A. T. (1994). *Introduction to fluid mechanics*: John Wiley.

Green, A. M. V. (2016). *Regulatory status Norway*. Paper presented at the Produced Water Management 2016, Stavanger.
Happel, J. (1958). Viscous flow in multiparticle systems: slow motion of fluids relative to beds of spherical particles. *AIChE Journal, 4*(2), 197-201.
Herzig, J., Leclerc, D., & Goff, P. L. (1970). Flow of suspensions through porous media—application to deep filtration. *Industrial & Engineering Chemistry, 62*(5), 8-35.
Hiemenz, P. C., & Rajagopalan, R. (1997). *Principles of Colloid and Surface Chemistry, revised and expanded* (Vol. 14): CRC press.
Hofsaess, T., & Kleinitz, W. (2003). *30 Years of Predicting Injectivity after Barkman & Davidson: Where are we today?* Paper presented at the SPE European Formation Damage Conference.
Hunter, R. (1987). Foundations of Colloid Science Clarendon. *New York*, 244-250.
Hunter, R. J. (2001). *Foundations of colloid science*: Oxford University Press.
Ison, C., & Ives, K. (1969). Removal mechanisms in deep bed filtration. *Chemical Engineering Science, 24*(4), 717-729.
Johnsen, S., Frost, T., Hjelsvold, M., & Utvik, T. R. (2000). *The Environmental Impact Factor-a proposed tool for produced water impact reduction, management and regulation.* Paper presented at the SPE International Conference on Health, Safety and Environment in Oil and Gas Exploration and Production.
Khatib, Z. (1994). *Prediction of formation damage due to suspended solids: Modeling approach of filter cake buildup in injectors.* Paper presented at the SPE Annual Technical Conference and Exhibition.
Khatib, Z., & Verbeek, P. (2003). Water to value-produced water management for sustainable field development of mature and green fields. *Journal of Petroleum Technology, 55*(01), 26-28.
Kraemer, T. F., & Reid, D. F. (1984). The occurrence and behavior of radium in saline formation water of the US Gulf Coast region. *Chemical geology, 46*(2), 153-174.
Neff, J., Lee, K., & DeBlois, E. (2011). *Produced water*: Springer.
Neff, J., Lee, K., & DeBlois, E. M. (2011). Produced water: overview of composition, fates, and effects *Produced water* (pp. 3-54): Springer.
Neff, J. M. (1987). *Biological effects of drilling fluids, drill cuttings and produced waters*: Elsevier Applied Science, London, United Kingdom.
Neff, J. M. (2002). *Bioaccumulation in marine organisms: effect of contaminants from oil well produced water*: Elsevier.
Pang, S., & Sharma, M. M. (1997). A model for predicting injectivity decline in water-injection wells. *SPE Formation Evaluation, 12*(03), 194-201.
Perkins, T., & Gonzalez, J. (1985). The effect of thermoelastic stresses on injection well fracturing. *Society of Petroleum Engineers Journal, 25*(01), 78-88.
Pillard, D. A., Tietge, J. E., & Evans, J. M. (1996). Estimating the acute toxicity of produced waters to marine organisms using predictive toxicity models *Produced Water 2* (pp. 49-59): Springer.
Reid, D. (1983). *Radium in formation waters: How much and is it of concern.* Paper presented at the 4th Annual Gulf of Mexico Information Transfer Meeting, New Orleans, LA. US Dept. of the Interior, Minerals Management Service, Gulf of Mexico OCS Office, New Orleans, LA.
Rubin, G. (1977). *Widerstands-und Auftriebsbeiwerte von ruhenden, kugelförmigen Partikeln in stationären, wandnahen, laminaren Grenzschichten*: na.
Sharma, M. M., & Pang, S. (1997). A model for predicting injectivity decline in water-injection wells. *SPE Formation Evaluation, 12*(03), 194-201.

Sharma, M. M., Pang, S., Wennberg, K. E., & Morgenthaler, L. (1997). *Injectivity decline in water injection wells: An offshore Gulf of Mexico case study.* Paper presented at the SPE European Formation Damage Conference.

Taylor, J. R., & Cohen, E. (1998). An introduction to error analysis: the study of uncertainties in physical measurements. *Measurement Science and Technology, 9*(6), 1015.

Terrens, G., & Tait, R. (1994). Effects on the marine environment of produced formation water discharges from offshore development in Bass Strait, Australia. *APEA JOURNAL, 34*, 730-730.

Tipura, L., Tjomsland, T., & Fagerbakke, A.-K. (2013). *Increasing Oil Recovery on the Grane Field With Challenging PWRI.* Paper presented at the OTC Brasil.

Tran, T., & Van den Broek, W. (1998). *Permeability decrease of sandstone as a result of injection of oil-and solids-containing water.* (Master), Delft University of Technology.

Trettin, D. R., & Doshi, M. R. (1980). Limiting flux in ultrafiltration of macromolecular solutions. *Chem. Engng Commun, 4*, 507-522.

Van den Broek, W., Bruin, J., Tran, T., Van der Zande, M., & Van der Meulen, H. (1999). *Core-flow experiments with oil and solids containing water.* Paper presented at the European formation damage conference.

Von Flatern, R. (2003). Troll pilot sheds light on seabed separation. *Offshore engineer*(MAI), 45-46.

Wennberg, K., & Sharma, M. (1997). *Determination of the filtration coefficient and the transition time for water injection wells.* Paper presented at the SPE European Formation Damage Conference.

Wolff, E. A. (2000). *Reduction of Emissions to Sea by Improved Produced Water Treatment and Subsea Separation Systems.* Paper presented at the SPE International Conference on Health, Safety and Environment in Oil and Gas Exploration and Production.

Wooding, R., & Chapman, T. (1966). Groundwater flow over a sloping impermeable layer: 1. Application of the Dupuit-Forchheimer assumption. *Journal of Geophysical Research, 71*(12), 2895-2902.

A. Appendix

Method of least square fit

The method of least square fit is performed when we have a series of data points where we would expect a linear relation:

$$y = a + bx \qquad \textit{Equation A.1}$$

Where x and y are two physical variables, while a and b are constants. This gives a linear relationship where the slope is represented by b and the a is the intersection with the y-axis.

If there were no uncertainties, each of the points would lie exactly on the curve $y = a + bx$. An example on this ideal relationship can be seen in Figure A.1, but a more realistic example where data points can be seen in Figure A.2 with their error bars (Taylor & Cohen, 1998).

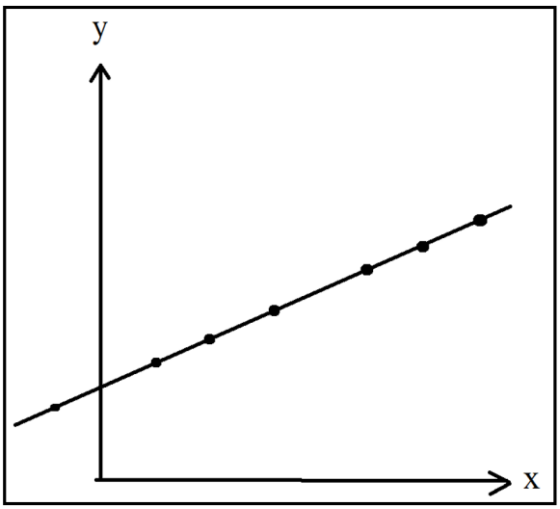

Figure A.1 Perfect linear relation

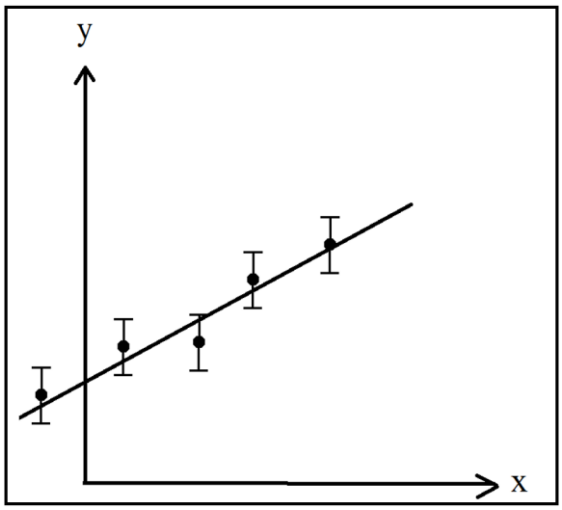

Figure A.2 Linear relation with uncertainties

The problem is to find a linear relation that best fits the data points. One of the most accepted model of finding the linear relationship is the method of least square fit.

We start with a set of measured data points $(x_1, y_1), \ldots\ldots, (x_N, y_N)$. The uncertainty in the measurement of x is assumed negligible. This is a reasonable assumption as there usually is one variable with much higher uncertainty. Another assumption is that the uncertainty in y all have the same magnitude, and that each measurement of y_i is governed by the Gauss distribution with the same standard deviation. We can compute the true value of y_i to a corresponding x_i value if we know the constants a and b.

As the measurement of the data point y_i is governed by a Gauss distribution with the true value at the centre and with equal to the standard deviation, σ_y. The probability of the observed value therefore be expressed as:

$$Prob_{a,b}(y_i) \propto \frac{1}{\sigma_y} e^{-\frac{(y_i-a-bx_i)^2}{2{\sigma_y}^2}} \qquad \textit{Equation A.2}$$

The probability of obtaining our set of data will then be equal to the product of the probability of all separate measured data points (Taylor & Cohen, 1998).

$$Prob_{A,B}(y_1, \dots, y_N) = \prod Prob_{A,B}(y_i) \propto \frac{1}{{\sigma_y}^N} e^{-\frac{\chi^2}{2}} \qquad \textit{Equation A.3}$$

Where

$$\chi = \sum_{i=1}^{N} \frac{(y_i - a - bx_i)^2}{{\sigma_y}^2} \qquad \textit{Equation A.4}$$

We will then assume that the best estimate of A and B will be when the Probability $Prob_{A,B}(y_1, \dots, y_N)$ is maximum. From the formulas above we can see that the probability is maximum when χ^2 is minimum. This is the reason that this method is called the least square method. We differentiate χ^2 with respect to A and B and set the derivative equal to zero to

$$\frac{\delta\chi^2}{\delta a} = -\frac{2}{{\sigma_y}^2}\sum_{i=1}^{N}(y_i - a - bx_i) = 0 \qquad \textit{Equation A.5}$$

$$\frac{\delta\chi^2}{\delta a} = -\frac{2}{{\sigma_y}^2}\sum_{i=1}^{N}x(y_i - a - bx_i) = 0 \qquad \textit{Equation A.6}$$

find the minimum value of χ^2 (Taylor & Cohen, 1998).

These two equation can be rewritten as:

$$aN + b\sum x_i = \sum y_i \qquad \textit{Equation A.7}$$

$$a\sum x_i + b\sum {x_i}^2 = \sum x_i y_i \qquad \textit{Equation A.8}$$

We now have two equations with two unknowns. We can now solve this equation with respect to A and B:

$$a = \frac{\sum {x_i}^2 \sum y_i - \sum x_i \sum x_i y_i}{N\sum {x_i}^2 - (\sum x_i)^2} \qquad \textit{Equation A.9}$$

$$b = \frac{N\sum x_i y_i - \sum x_i \sum y_i}{N\sum {x_i}^2 - (\sum x_i)^2} \qquad \textit{Equation A.10}$$

Using Equation A.9 and Equation A.10 to calculate A and B we get the best estimate of the straight line according the method of least square fit (Taylor & Cohen, 1998).